

Matthias Rath, BSc

Sensor Modeling and Optimization for Capacitive Ice Sensing

MASTER'S THESIS

to achieve the university degree of
Diplom-Ingenieur
Master's degree program: Electrical Engineering

submitted to
Graz University of Technology

Supervisor
Dipl.-Ing. Dr.techn Markus Neumayer

Institute of Electrical Measurement and Measurement Signal Processing

Faculty of Electrical and Information Engineering

Graz, September 2016

Affidavit

I declare that I have authored this thesis independently, that I have not used other than the declared sources/resources, and that I have explicitly indicated all material which has been quoted either literally or by content from the used sources. The text document uploaded to TUGRAZonline is identical to the present master's thesis.

Date

Signature

Eidesstattliche Erklärung

Ich erkläre an Eides statt, dass ich die vorliegende Arbeit selbstständig verfasst, andere als die angegebenen Quellen/Hilfsmittel nicht benutzt, und die den benutzten Quellen wörtlich und inhaltlich entnommenen Stellen als solche kenntlich gemacht habe. Das in TUGRAZonline hochgeladene Textdokument ist mit der vorliegenden Masterarbeit identisch.

Datum

Unterschrift

Abstract

Natural ice formation in cold climate regions poses a risk to technical systems, which operate outdoors. Sensing systems are needed to detect and measure ice accretion. Among other sensing principles, capacitive approaches for ice sensing have been proven viable for this application and have been implemented. In capacitive sensing, the information of interest is derived from capacitance measurements. As an indirect sensing system, it has to distinguish between ice and water exclusively by their dielectric properties. However, the dielectric properties of ice and water can also depend on the environmental conditions, for example, temperature and humidity. Furthermore, the form of ice and rain on the sensor is also of random nature. The stochastic behavior of this process has to be considered in the design of such sensors. In this thesis, capacitive sensing of ice is investigated with particular considerations concerning the random nature of ice and rain scenarios. The dielectric properties of ice were studied using laboratory experiments as well as an existing capacitive ice sensor. All results were incorporated in a general framework for sensor simulation and optimization. It provides methods to simulate the behavior of different sensors for numerous ice and rain scenarios. These scenarios are stochastically generated to simulate the natural variations in ice and rain behavior. Different approaches for optimal sensor design will be discussed. For each approach, a design study was conducted using the framework.

Zusammenfassung

Natürliche Eisbildung stellt für den sicheren technischen Betrieb vieler Systeme ein Risiko dar. Zur frühzeitigen Erkennung von gefährlichen Zuständen der Eislast werden Messsysteme benötigt, die den Zustand der Eisbildung sensorisch erfassen. Die kapazitive Messtechnik hat sich hierzu als besonders geeignet erwiesen. Kapazitive Messverfahren basieren auf der Auswertung von Messkapazitäten, die die eigentliche Messgröße indirekt abbilden. Für die sensorische Erfassung von Eis können die dielektrischen Eigenschaften von Wasser für verschiedene Aggregatzustände verwendet werden, welche zu einer Änderung der Messkapazitäten führen. Die dielektrische Permittivität von Eis unterliegt jedoch gewissen Schwankungen, was im Grenzübergang der Eisbildung eine zuverlässige sensorische Erfassung und Unterscheidung von Wasser erschwert. So können die dielektrischen Eigenschaften von Eis von der Temperatur und der Umgebungsfeuchte abhängen. Ebenso ist die Eisbildung auf einem Sensor nicht deterministisch, sondern besitzt ein stochastisches Verhalten. In dieser Arbeit werden Konzepte zum Entwurf kapazitiver Eissensorik erarbeitet, die besonders auf die zufällige Natur des Vereisungsprozesses Rücksicht nehmen. In Laborexperimenten und mit Hilfe existierender Sensorik wurden die dielektrischen Eigenschaften von Eis für eine kapazitive Sensoranwendung untersucht. Für den Entwurf neuer Sensoren wurde ein Simulations-Framework erstellt, das eine Untersuchung der Sensoreffekte unter Berücksichtigung der Effekte bei natürlicher Eisbildung erlaubt. Unter Anwendung dieses Frameworks werden Optimierungsstrategien für den Entwurf optimaler Sensor-Layouts entwickelt und diskutiert.

Contents

1	Introduction	1
1.1	Motivation	1
1.2	Overview of Existing Methods for Ice Sensing	2
1.2.1	Force-Based Sensing	2
1.2.2	Optical Sensing	3
1.2.3	Capacitive Sensing	3
1.3	Ice Measuring at the EMT With Capacitive Ice Sensors	6
1.4	Aim of this Thesis	7
1.4.1	Modeling of a Capacitive Sensor System	9
1.4.2	Optimal Sensor Design and Sensor Signal Processing	10
1.4.3	Detection of Ice	10
1.4.4	Thickness Estimation of Ice	11
1.5	Outline of this Thesis	12
2	Modeling Capacitive Sensor Effects for Ice Sensors	13
2.1	Modeling of Capacitive Sensors	14
2.1.1	Boundary Conditions	18
2.1.2	Capacitance Evaluation	19
2.2	Analysis of the Prototype Capacitive Ice Sensor	21
2.2.1	Electrode Layout	21
2.2.2	Capacitive Sensing Circuitry	21
2.2.3	3D-FEM-Simulation Study	23
2.2.4	Sensitivity Map Analysis	25
2.2.5	Ice Layer Thickness Experiment	31
2.3	Dielectric Properties of Water and Ice	34
2.3.1	Coaxial Permittivity Probe	35
2.3.2	Ice Properties from Capacitive Measurements	40
2.3.3	Coverage Properties of Ice	44
2.4	Summary	44

Contents

3	Sensor Simulation Framework	47
3.1	Generic Sensor Simulation Model	48
3.1.1	Electrodes	50
3.1.2	Region of Interest	52
3.1.3	Ground Plane	53
3.1.4	Insulation Layers	53
3.1.5	Far Boundary Box	54
3.2	Rain and Ice Pattern Generation	54
3.2.1	Material Mapping	55
3.2.2	Pattern Prototypes	57
3.2.3	Pattern Statistic	58
3.2.4	Rain Patterns	59
3.2.5	Ice Patterns	63
3.3	Complete Simulation Process	70
3.3.1	Post-Processing of Capacitance	71
3.4	Complete Optimization Process	71
3.5	Summary	73
4	Design of Optimized Sensors	75
4.1	Ice Detector Design	76
4.1.1	Binary Classification	78
4.1.2	Objective Function	80
4.1.3	Computational Steps	81
4.2	Linear Ice Sensor Design with One Capacitance	81
4.2.1	Objective Function	84
4.2.2	Computational Steps	84
4.3	Linear Ice Sensor Design with Multiple Capacitances	84
4.3.1	Objective Function	86
4.3.2	Computational Steps	86
4.4	Combined Sensor/Algorithm Design	87
4.4.1	Optimal Approximation as a General Estimator	87
4.4.2	Objective Function	91
4.4.3	Computational Steps	91
4.5	Summary	92
5	Design Studies	93
5.1	General Prototype Considerations	93

5.2	Ice Detector Design	95
5.2.1	Optimization Result	96
5.3	Linear Ice Thickness Sensor Design	99
5.3.1	Optimization Result	101
5.4	Combined Sensor/Algorithm Design	104
5.4.1	Transmitter Current Consideration	105
5.4.2	Optimization Result	106
6	Conclusion and Outlook	111
6.1	Conclusion	111
6.2	Outlook	113
6.2.1	Confirmation of the Simulation Results and Construction of a Prototype	113
6.2.2	Different Objective Functions	113
6.2.3	Deeper Study of Ice Patterns	114
	Bibliography	115

List of Figures

1.1	Plate capacitor.	4
1.2	Plate capacitor bent open for ice measurement.	5
1.3	Ice detector electrode setup directly on the wire.	7
1.4	Capacitive ice sensor for monitoring ice accretion [12].	8
1.5	Results of a neuronal network ice indicator for an outdoor experiment [12].	9
2.1	Modeling scheme for an impedance sensor.	14
2.2	Probe and electrode setup of the prototype capacitive ice sensor [12].	22
2.3	Cross-section of the prototype capacitive ice sensor.	22
2.4	3D-view of a section of the sensor model with one raindrop on the surface.	24
2.5	3D-view of the sensor model with the grid of possible cuboid locations.	24
2.6	3D-view of the sensor model with an ice layer.	24
2.7	Capacitance sensitivity map of electrode 1 for ice.	27
2.8	Capacitance sensitivity map of electrode 2 for ice.	28
2.9	Capacitance sensitivity map of electrode 4 for ice.	29
2.10	Capacitance sensitivity map of electrode 3 (ring) for ice.	30
2.11	Capacitance sensitivity map of electrode 3 (ring) for water.	31
2.12	Sensor readings for PMMA layers of different thickness.	32
2.13	Normalized sensor readings for PMMA layers of different thickness.	32
2.14	Normalized simulated sensor readings for ice layers of different thickness.	33
2.15	Photo of the coaxial capacitance probe with connection wires.	36
2.16	Drawing of the coaxial capacitance probe with its dimensions.	36

List of Figures

2.17	Capacitances of the coaxial capacitance probe connected in series.	37
2.18	Relative permittivity of freezing ice over time at -15°C . . .	39
2.19	Relative permittivity of thawing ice over time at 20°C	39
2.20	Sensor behavior for dry and wet ice.	41
2.21	Simulated sensor behavior for deep-frozen ice of increasing thickness	41
2.22	Picture of the ice layer on the sensor right before the heating cycle.	42
2.23	Factors of simulated sensor reading increase for different ϵ_r at 5.4 mm ice layer thickness.	44
3.1	Measurement system of the ice sensor.	48
3.2	Flowchart of the optimization process.	49
3.3	Illustration of the generic sensor model for four electrodes.	50
3.4	Mesh of the sensor, zoomed to an electrode.	51
3.5	Rounded corners of an electrode in the mesh.	52
3.6	Mesh of a sensor and simulation region.	53
3.7	Ice scenario on a generic sensor.	54
3.8	Mapping of a pattern onto the Region of Interest.	56
3.9	Pattern prototype for a single block of ice.	57
3.10	Example of a pattern "Four Raindrops".	60
3.11	Example of a pattern "Variable Number of Raindrops".	61
3.12	Example of a pattern "Thin Film of Water of Variable Thickness".	62
3.13	Example of a pattern "Deep-Frozen Ice Layer of Varying Thickness Covering the Whole Sensor".	64
3.14	Example of a pattern "Wet Ice Layer of Varying Thickness Covering the Whole Sensor".	65
3.15	Example of a pattern "Deep-Frozen Ice of Varying Thickness Covering Half the Sensor".	66
3.16	Example of a pattern "Wet Ice of Varying Thickness Covering Half the Sensor".	67
3.17	Example of a pattern "Wet Ice of Varying Thickness Unevenly Covering the Sensor".	68
3.18	Example of a pattern "Thin, Wet Ice Layer of Varying Thickness Covering the Whole Sensor".	69

List of Figures

4.1	Thresholds of the ice detector.	77
4.2	Receiver Operating Characteristic.	79
4.3	Combined linear behavior of multiple capacitances.	85
4.4	Flowchart of the optimization process, expanded by the combined sensor/algorithm design.	88
5.1	General layout of a prototype PCB.	94
5.2	Generic model of the detector electrodes' geometries.	95
5.3	Prototype layout of the optimized detector design and a hand-drawn design.	97
5.4	Receiver Operating Characteristic of the ice detector.	98
5.5	Histograms of simulated sensor values for ice and rain and the optimal threshold.	99
5.6	Generic model of the sensing electrodes' geometries.	100
5.7	Prototype layout of the optimized linear ice thickness sensor design and a hand-drawn design.	102
5.8	Simulated electrode behavior depending on the ice thickness (optimized).	102
5.9	Simulated combined electrode behavior depending on the ice thickness (optimized).	103
5.10	Simulated electrode behavior depending on the ice thickness (hand-drawn).	103
5.11	Prototype layout of the ice thickness sensor optimized by the combined sensor/algorithm design and a hand-drawn design.	106
5.12	Averaged performance of the sensor and algorithm.	107
5.13	Linear fit to the performance of the sensor and algorithm.	108
5.14	Standard deviation of the sensor and algorithm.	109

1 Introduction

1.1 Motivation

Natural ice accretion can interfere with everyday technical applications in cold climate regions in different ways [1]. Atmospheric ice can form when the right conditions are met. At low enough temperatures, humidity from rain or even humid air can form ice layers of varying thickness [2]. Critical surfaces can be defined as those surfaces where the effects of ice accretion cannot be neglected. Ice accretion either makes surfaces slippery, or adds unwanted weight, thus creating dangerous situations. This applies to technical systems and structures operating outdoors, like overhead power transmission lines or wind turbine blades. The effects of ice forming on critical surfaces have to be taken into consideration when designing such systems.

One type of critical surface where ice monitoring is of importance is the wire of an overhead power transmission line. The additional weight on the wire could potentially damage the wire or even lead to the collapse of the supporting towers, creating threats for humans and properties [3]. Power grid companies seek a reliable way to receive an early warning when ice accretion starts, as well as to estimate the amount of ice on the line. This motivates the design of an ice sensor that can detect ice and also estimate its mass and therefore the potential for danger. On a given constant area of a critical surface, the thickness of the ice layer is a measure for its mass when the surface is evenly covered. This leads to implementations of thickness sensors to assess the threat potential of ice.

Depending on the thickness of the ice, different countermeasures can be initiated. For thin ice layers which have just started to form, it might suffice to remotely melt the ice. This is done by routing more of the power

1 Introduction

grid traffic over that line to effectively warm it up due to thermal losses and therefore melt the ice before a dangerous amount can build up. In case of a larger ice buildup, human interaction is required to remove the ice to avoid damage [4].

The next section will give an overview of methods that have been proposed to sense the ice mass on critical surfaces.

1.2 Overview of Existing Methods for Ice Sensing

This section presents a short overview of different approaches for ice detection and mass or thickness measurement. It focuses on methods which are used on overhead power transmission lines. Methods which are mainly used for large scale ice thickness measurements on glaciers and on ocean ice formations are therefore excluded. Several different approaches have already been proposed to measure ice on overhead power transmission lines:

- Force-based sensing.
- Optical sensing.
- Capacitive sensing.

Each approach offers a distinct list of advantages and disadvantages which are discussed.

1.2.1 Force-Based Sensing

The danger potential of ice on power transmission lines can be assessed by measuring the force acting on the support towers through the wires and therefore the mass of the ice. Force sensors have to be installed at the supporting towers, so it is not possible to measure the icing situation on different places on the wire. Without further measurements, the sensor cannot distinguish whether the additional load is caused by ice or snow.

1.2 Overview of Existing Methods for Ice Sensing

There are other factors that influence the measurement, like the force the wind exerts on the wire. To compensate those influences in the estimate of the ice mass, those parameters have to be measured too [5]. Although the additional mass is the parameter of interest for assessing the damage potential it is also useful to know the thickness of the ice layer on the wire to initiate the appropriate countermeasure. This is complicated to achieve from mass measurements alone because the distribution of ice on the wire is not known. A method to estimate the thickness from the measured mass and the influencing parameters is presented in [6].

1.2.2 Optical Sensing

One optical approach is to use cameras to film the icing on the power transmission wires. Image processing is used to generate an automated measurement of the ice thickness. An advantage of this method is that in addition to the measurement, a visual monitoring by humans is possible to remotely judge critical situations when they arise. On the other hand, there is the drawback of low light performance which comes with a camera application. This creates the need for illumination and leads to a greater power consumption, making it not a viable option for wireless operation. Additionally, ice buildup on the camera itself could obstruct its vision. A monitoring system powered by photo voltaic panels has been presented in [7].

A second optical approach to ice sensing is utilizing the refraction properties of ice. Light is guided from a source into the ice volume by optic fibers. Depending on the ice, the light will be transmitted or reflected. The reflected light is measured and used to derive information, like its thickness, about the ice [8].

1.2.3 Capacitive Sensing

The capacitive sensing principle is widely used for various sensor applications [9].

1 Introduction

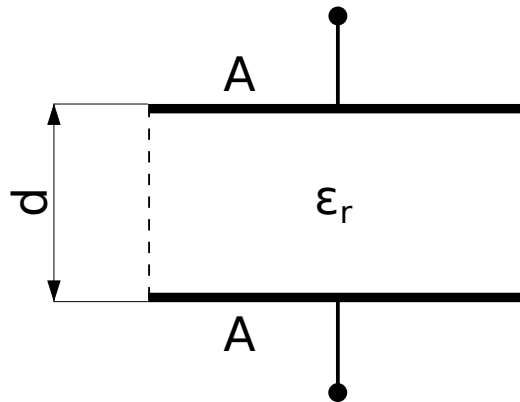


Figure 1.1: Plate capacitor.

The basic principle of a capacitive sensor setup for thickness measurement can be explained with the parallel plate capacitor illustrated in figure 1.1 [9]. The capacitance of the plate capacitor is given by

$$C = \epsilon_0 \epsilon_r \cdot \frac{A}{d}. \quad (1.1)$$

By varying the parameters in (1.1), it is possible to measure the distance by the capacitance C . The area in which the plates overlap is denoted by A and the distance of the plates from each other by d . ϵ_0 thereby denotes the permittivity of vacuum, and ϵ_r the relative permittivity of the dielectric medium in the capacitor.

In the setup illustrated in the sketch in figure 1.1, two conducting plates, which are insulated from each other, form the capacitor. Both plates can be moved and are separated by an insulating medium with the relative permittivity ϵ_r . Moving the plates vertically to increase the distance d decreases the capacitance C . Likewise, a movement in the horizontal direction decreases the overlapping area A , which effectively forms the capacitor, and in turn decreases the capacitance C . If one plate is kept stationary and the other plate is linked to a moving part representing the distance to be measured, the change in capacitance can be used to calculate the change in distance.

1.2 Overview of Existing Methods for Ice Sensing

Another way to vary the capacitance C of a basic plate capacitor is to change the relative permittivity ϵ_r . This could be done by introducing another material with a different permittivity ϵ_r from the usual insulating medium. The amount of the second material is linked to the distance to be measured. Then the change in capacitance can again be used to calculate this distance. Since now multiple relative permittivities are involved, the basic formula (1.1) is not applicable anymore.

Using the change in capacitance due to the change in dielectric properties provides a suitable measurement principal for a capacitive ice sensor. Since it is impractical to have any moving part linked to the ice, instead the change in permittivity is used to detect ice or measure its thickness. It is also impractical to have the two plates mounted above each other like in the model of the plate capacitor. This would interfere with the natural forming of ice, potentially skewing the measurement. Instead, the parallel plate capacitor is bent open and its plates are mounted in the same plane as illustrated in figure 1.2. This means that the model used to describe the effect and the formula (1.1) cannot be applied to this case. For more complex distributions of materials with different permittivities, there is no formula to calculate the resulting capacitance. Nevertheless, the basic relations, like that a change in permittivity leads to a change in capacitance, still hold. Methods to solve the inverse problem of determining the material distribution from measured capacitances have been used in electrical capacitance tomography (ECT) and are described in [10].

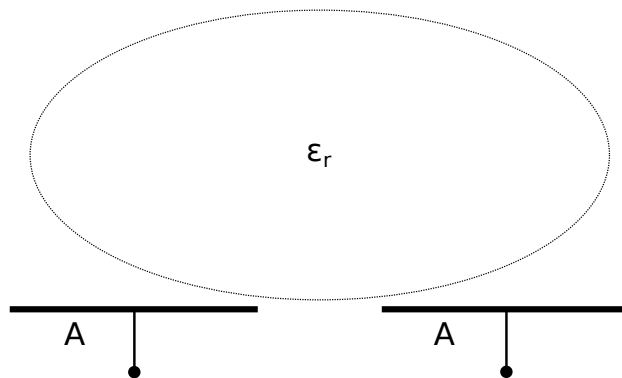


Figure 1.2: Plate capacitor bent open for ice measurement.

1 Introduction

In the planar setup, the electrode areas A and distance d are kept constant. The only possible variation left is through change in the relative permittivity ϵ_r of different materials covering the sensor. The different mediums involved in a cold climate outdoors scenario are air, water, and ice. They each differ in permittivity, making it possible for the described principle to work. If the area above the plates is now covered in an ice layer, the measurement of the capacitance C can be used to detect ice and estimate the ice layer thickness. The thickness is then used as an indicator for the total additional mass on the power transmission line.

A capacitive sensor working in the described way is very versatile. It is not influenced by wind like the force measurement, or dependent on light like a camera. Since it consumes little power, it can be built to operate wireless. This enables locally specific measurements by placing the sensor on the power line itself. An icing detector using this principle has been described in [11].

1.3 Ice Measuring at the EMT With Capacitive Ice Sensors

Ice sensing using capacitive sensing principles has seen a long research history at the Institute of Electrical Measurement and Measurement Signal Processing (EMT).

First feasibility studies were conducted around the year 2008 and presented in [11]. The detector described in this paper used sensing electrodes which were mounted directly on the power transmission line. Its electrode setup is sketched in figure 1.3.

Figure 1.4 shows a picture of a sensor prototype for capacitive ice monitoring [12]. This sensor is targeted at ice detection and thickness measurements on overhead high voltage power lines with a casing designed for the particular requirements regarding high voltages. Results for experiments conducted outdoors during wintertime are shown in figure 1.5 where a neuronal network approach is used to analyze the presence of ice. Measurement data acquired with this prototype yields viable information

1.4 Aim of this Thesis

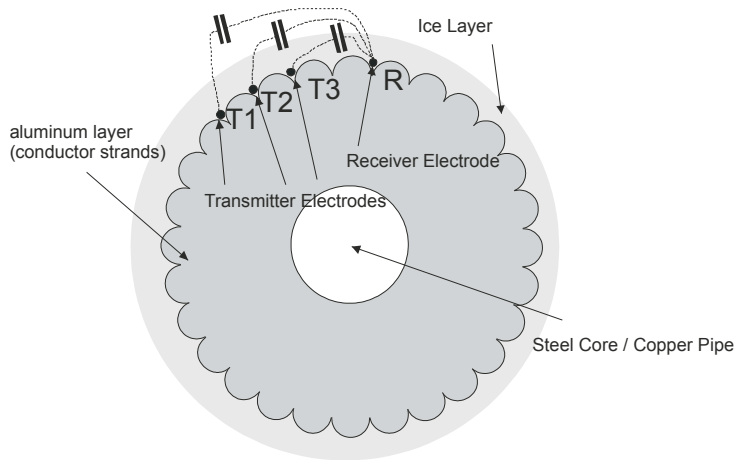


Figure 1.3: Ice detector electrode setup directly on the wire [11].

about the behavior of ice on a sensor. This prior knowledge is needed for the design of a new sensor.

Different reconstruction algorithms for detecting ice and estimating its thickness were developed. A reconstruction method using a neuronal network is mentioned in [12]. Learning-based algorithms use the measurement data without any knowledge of the underlying model. The paper describes a model-based approach and its potential and feasibility.

1.4 Aim of this Thesis

The capacitive sensor effect for ice measurement has been demonstrated and implemented in a prototype ice sensor. Its electrode geometry is not optimal, though. This thesis aims to implement a sensor model for a planar capacitive ice sensor. With this model, it is possible to simulate the sensor behavior. Repeated simulation can then be used in an optimization process to find the optimal electrode geometry. To keep the modeling, simulation and optimization processes versatile, a framework incorporating all the single steps will be built. Details on the main goals of the thesis are given in the following sections.

1 Introduction

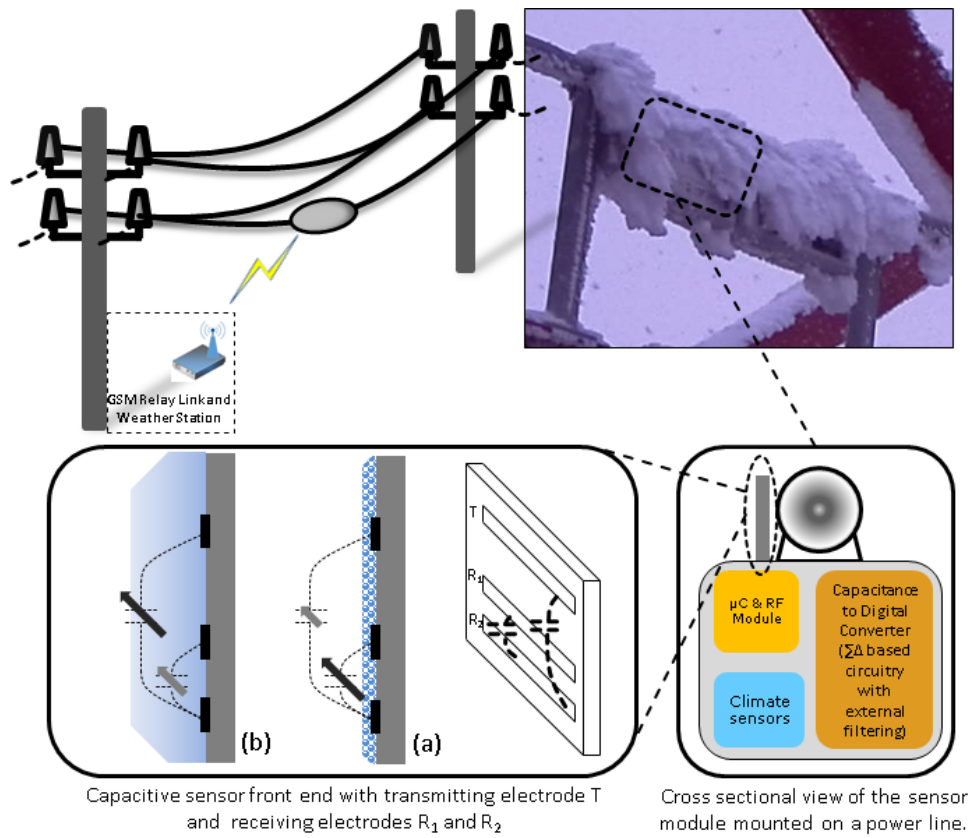


Figure 1.4: Capacitive ice sensor for monitoring ice accretion [12].

1.4 Aim of this Thesis

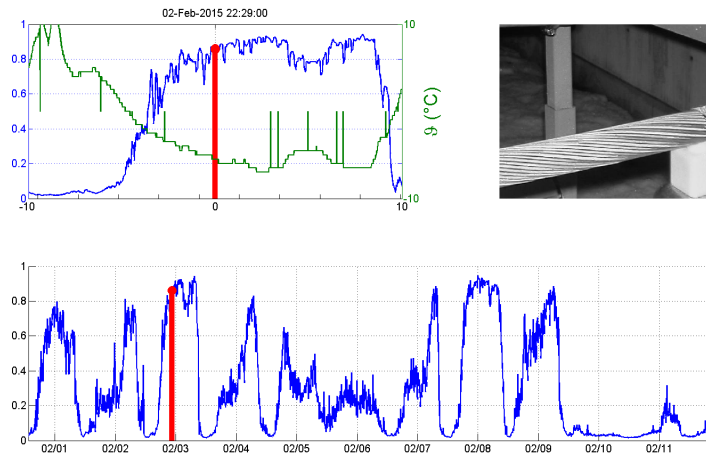


Figure 1.5: Results of a neuronal network ice indicator for an outdoor experiment [12].

1.4.1 Modeling of a Capacitive Sensor System

The first goal of this thesis is to implement a sensor model for a capacitive ice sensor. This model has to include a variable electrode geometry as well as a method to implement different icing and rain scenarios. It is important to have a model with variable geometry to eventually find the best electrode layout with an optimization algorithm. The ice and rain scenarios will be used to simulate the behavior of the sensor under different situations and to assess its performance. To implement those scenarios, the dielectric properties, especially of ice, have to be analyzed. The following subsection discusses the individual goals.

Dielectric Properties of Ice

To design a simulation environment for detecting icing events and measuring the thickness of ice layers, knowledge about the dielectric properties of ice is crucial. Of special interest is the behavior of the permittivity of ice at different temperature and moisture levels. To get these parameters for the simulations, measurements in a climatic chamber with a probe have to be made. Previous measurements from a prototype capacitive ice sensor have to be analyzed. Other observations from experiments with the sensor,

1 Introduction

both outside and inside the climatic chamber, should lead to insight about the form of ice layers. This knowledge is then used to design different icing pattern for use in the simulations.

1.4.2 Optimal Sensor Design and Sensor Signal Processing

With the help of the established sensor model, planar capacitive ice sensors of different geometries can be simulated. The observed properties of ice can be used to replicate real world ice patterns in these simulations. Through evaluation of the simulations' results, the electrode layout can be optimized for specific parameters before a prototype is built.

The main requirements to an ice sensor are:

- Ice detection.
- Ice mass estimation.

Ice mass estimation will be done through measuring the thickness of the ice layer on the sensor. Those specifications require different strategies in the optimization process which are discussed below.

1.4.3 Detection of Ice

The task of the ice detector is to distinguish between ice and water on the sensor surface. In the field application, the sensor has to distinguish between these two basic scenarios. Either it is too warm for ice to form and rainwater will collect on the sensor's surface, or it is cold enough for ice formation. Since rain will flow off the power transmission wires, there is no danger of high additional weight. Only ice forming thicker layers on this critical surface poses a threat. Therefore, the sensor first has to distinguish between these two situations before applying the thickness estimation algorithm. The detector will be optimized to distinguish between ice and rain.

1.4.4 Thickness Estimation of Ice

Whereas the ice detector mainly focuses on distinguishing ice from rain, the ice thickness sensor also estimates the thickness of the ice layer on the sensor. Different measures for the performance of a thickness sensor have to be found and formulated. Those measures include optimizing the sensor for a linear behavior as well as an approach where the sensor geometry is optimized together with its estimation algorithm.

1.5 Outline of this Thesis

This section gives a short overview of the topics to be discussed in the individual chapters.

In chapter 2, Modeling Capacitive Sensor Effects for Ice Sensors, the modeling of a capacitive sensor with the means of partial differential equations (PDE) is described. An existing prototype capacitive ice sensor is analyzed by measurements and simulations to gain knowledge about electrode layouts as well as the behavior of ice. Since the dielectric properties of ice are of special interest to create sensor simulations, those are further analyzed.

Chapter 3, Sensor Simulation Framework, deals with all the necessary steps to set up a framework for the simulations and optimization of a capacitive ice sensor. A generic model is introduced and a method for generating ice and rain patterns for the simulations is described. Furthermore, methods on how the patterns are mapped to the sensor model for a fast simulation are of special interest.

The chapter 4, Design of Optimized Sensors, describes the methods of optimization for an ice detector and for an ice sensor. It is discussed how the so-called objective functions are used to express these methods as a performance measure for further optimization.

In chapter 5, Design Studies, the framework is used to produce optimized electrode designs corresponding to the objective functions devised in chapter 4. The limiting parameters for the production of a prototype printed circuit board (PCB) were incorporated.

The last chapter 6 presents a final summary of the thesis as well as an outlook into further research topics.

2 Modeling Capacitive Sensor Effects for Ice Sensors

This chapter deals with the modeling of a capacitive sensor as well as analyzing the existing prototype capacitive ice sensor to learn about its properties. The sensor is then also used for ice measurements to study the dielectric properties of ice.

Capacitive sensing utilizes measured capacitances to draw conclusions about the behavior of some underlying quantity [12]. To create a reliable simulation of a capacitive ice sensor, the underlying principles have to be understood. Therefore a short recap of the basics of electrostatics with a focus on capacitance evaluation is given.

A problem with indirect measurements are all the additional factors that influence the permittivity or the capacitance besides the parameter that should be measured. A good sensor design should minimize those unwanted cross sensitivities while maximizing the influence of the parameter to be measured, which is the thickness of the ice layer. A multi-electrode approach is used to combine different sensitivity characteristics in one sensor and minimize the influence of cross sensitivities. This will lead to smaller measurement uncertainty and better estimation performance of the ice thickness [13].

An important part in this chapter concerns the collection of prior knowledge about rain and ice. Neither water nor ice have just one fixed value for their permittivity. Their distributions on the sensor are also always different. The permittivity of a material can change with frequency. In the case of ice, it can change with the content of unfrozen water or the wetness of the ice. This knowledge can then later be incorporated into the

2 Modeling Capacitive Sensor Effects for Ice Sensors

optimization process. Together with the uneven nature of ice layers, those are the greatest problems to be solved.

Experimental observations of rain and ice, the two mediums relevant for the sensing scenario, are provided. Since the measuring hardware from the existing prototype capacitive ice sensor was reused, its features and limitations are discussed. This chapter concludes with an analysis of the electrode setup of the sensor.

2.1 Modeling of Capacitive Sensors

In this section, the governing partial differential equations (PDE) of the capacitive sensor model are discussed. The model of the capacitive sensor is derived from Maxwell's equations [14]. Some simplifications described in [15] are made to create an electrostatic formulation. The goal is to find a PDE, which can be solved for the capacitance C between two electrodes.

In the illustration in figure 2.1 the basic problem setup and its boundaries are sketched. Two electrodes with the surfaces Γ_{E11} and Γ_{E12} and the complex impedance Z between them are shown. Part of the complex impedance Z is the capacitance C of interest. The surfaces $\partial\Omega_1$ and $\partial\Omega_2$ describe the boundaries of the modeling region.

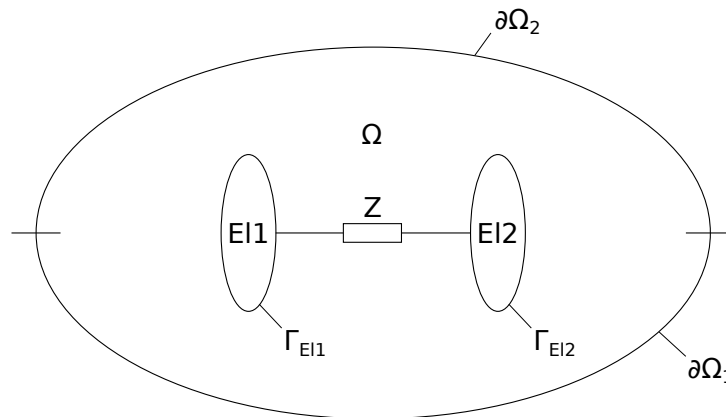


Figure 2.1: Modeling scheme for an impedance sensor.

2.1 Modeling of Capacitive Sensors

Since the modeling equations are based on Maxwell's equations with selected simplifications and boundary conditions, a summary of Maxwell's equations follows.

Maxwell's first equation

$$\nabla \cdot \vec{\mathbf{D}} = \rho, \quad (2.1)$$

is Gauss' Law, which identifies the electric charge density ρ as the source of the electric flux density $\vec{\mathbf{D}}$. The second Maxwell equation is Gauss' Law of Magnetism expressed by

$$\nabla \cdot \vec{\mathbf{B}} = 0, \quad (2.2)$$

which states that there are no magnetic charges which could be sources to the magnetic flux density $\vec{\mathbf{B}}$.

Equations three and four are

$$\nabla \times \vec{\mathbf{E}} = -\frac{\partial \vec{\mathbf{B}}}{\partial t}, \quad (2.3)$$

and

$$\nabla \times \vec{\mathbf{H}} = \frac{\partial \vec{\mathbf{D}}}{\partial t} + \vec{\mathbf{J}}, \quad (2.4)$$

and are called Faraday's Law of Induction and Ampere's Law, respectively. Faraday's Law of Induction states that the change over time of the magnetic flux density $\vec{\mathbf{B}}$ is the cause for the curls of the electric field $\vec{\mathbf{E}}$. This is used to explain the generative principle. Similarly, Ampere's Law describes the cause of curls in the magnetic field $\vec{\mathbf{H}}$. $\vec{\mathbf{J}}$ is the electric current density. The displacement current density also produces curls, but those are caused by the change over time of the electric flux density $\vec{\mathbf{D}}$.

The material relations

2 Modeling Capacitive Sensor Effects for Ice Sensors

$$\vec{\mathbf{D}} = \varepsilon \vec{\mathbf{E}}, \quad (2.5)$$

$$\vec{\mathbf{B}} = \mu \vec{\mathbf{H}}, \quad (2.6)$$

and

$$\vec{\mathbf{J}} = \sigma \vec{\mathbf{E}} \quad (2.7)$$

complement the Maxwell equations. Equation (2.7) expresses the relation of the current density $\vec{\mathbf{J}}$ to the electric field $\vec{\mathbf{E}}$ where σ is the conductivity. ε is the permittivity of the medium and can be split into

$$\varepsilon = \varepsilon_0 \varepsilon_r, \quad (2.8)$$

where ε_0 is the permittivity of a vacuum. ε_r is the relative permittivity of the medium used to describe the permittivity of a material in relation to ε_0 . The permeability in equation (2.6) is denoted by μ .

In order to simplify those equations, some assumptions are made. The sensor electronics transmitter typically operates at a relatively low frequency of 240 kHz and therefore the wavelength is far larger than any of the electrical structures involved. This implies that there are no wave propagation effects for the sensor. From that follows that the magnetic fields inside the sensor have no influences on the electric field. This is expressed by

$$\nabla \times \vec{\mathbf{E}} = -\frac{\partial \vec{\mathbf{B}}}{\partial t} = 0, \quad (2.9)$$

which is a simplification of Maxwell's third equation (2.3).

Since the electric field $\vec{\mathbf{E}}$ has no curl, the notion of the electric scalar potential V can be introduced, expressing the electric field as

$$\vec{\mathbf{E}} = -\nabla V. \quad (2.10)$$

2.1 Modeling of Capacitive Sensors

Applying the divergence operator to Ampere's Law (2.4) results in

$$\nabla \cdot (\nabla \times \vec{\mathbf{H}}) = \nabla \cdot \left(\vec{\mathbf{J}} + \frac{\partial \vec{\mathbf{D}}}{\partial t} \right) = 0 \quad (2.11)$$

because the divergence of a curl is always zero.

Applying the Fourier Transform results in a representation of the time derivative by $j\omega$ as

$$\nabla \cdot (\vec{\mathbf{J}} + j\omega \vec{\mathbf{D}}) = 0. \quad (2.12)$$

ω denotes the circular frequency, where $\omega = 2\pi f$.

Using the relation from (2.7), $\vec{\mathbf{J}}$ can be substituted by $\sigma \vec{\mathbf{E}}$. $\vec{\mathbf{D}}$ equals $\epsilon \vec{\mathbf{E}}$ as in material relation (2.5), which leads to

$$\nabla \cdot (\sigma \vec{\mathbf{E}} + j\omega \epsilon_0 \epsilon_r \vec{\mathbf{E}}) = 0. \quad (2.13)$$

With the scalar potential introduced in (2.10) this results in

$$-\nabla \cdot ((\sigma + j\omega \epsilon_0 \epsilon_r) \nabla V) = 0. \quad (2.14)$$

This is the PDE which can be used to simulate the electric effects for the sensor. The conductivity σ is still present in this equation.

It is assumed that the conductivity of rain water is negligible small and that there are no other conductive materials in the sensor's vicinity. The conductivity σ is therefore 0 resulting in

$$-\nabla \cdot (j\omega \epsilon_0 \epsilon_r \nabla V) = 0. \quad (2.15)$$

The equation further simplifies for a constant frequency ω to

$$\nabla \cdot (\epsilon_0 \epsilon_r \nabla V) = 0. \quad (2.16)$$

2 Modeling Capacitive Sensor Effects for Ice Sensors

When no charge density ρ is assumed in the area around the sensor, a similar result can be derived from the first of Maxwell's equations (2.1) when ρ is 0 which leaves

$$\nabla \cdot (\epsilon \vec{E}) = 0. \quad (2.17)$$

Substituting $-\nabla V$ for \vec{E} would result in the same equation as in (2.16). This differs from

$$\nabla \cdot \nabla V = \Delta V = 0, \quad (2.18)$$

which is Laplace's equation because ϵ_r is not a constant that can be neglected.

The finite element method (FEM) is used in this work to solve the PDE in equation (2.16). The scalar potential V is the result. From that, the charge distribution on the individual electrodes can be calculated and the capacitances can be computed.

2.1.1 Boundary Conditions

Boundary conditions are needed to solve the PDE (2.16) introduced in the previous section. In figure 2.1 two electrodes are shown. The model can be extended to any arbitrary number of electrodes which will be evaluated sequentially. To compute all cross capacitances in a multi-electrode setup, all electrodes have to be set active in turns.

In the following example electrode $E11$ is the active one. Dirichlet boundary conditions are used to describe the potential on the electrodes' surfaces. The potential V_0 is set for the active electrode and all other electrodes are set to a potential of 0 V as in

$$V_{\Gamma_{E11}} = V_0, \quad (2.19)$$

$$V_{\Gamma_{E12}} = 0. \quad (2.20)$$

2.1 Modeling of Capacitive Sensors

Γ_{E11} denotes the surface of electrode *E11* and Γ_{E12} the surface of electrode *E12* respectively.

Another boundary condition is needed to define the boundary of the model region. The model region boundary will influence the sensor and its behavior. To reduce the influence, a far boundary approach is used where the model region boundary is placed far away from the sensor. A Dirichlet boundary condition describes the fixed potential of the far boundary which is expressed by

$$V_{\partial\Omega_1} = 0, \quad (2.21)$$

and

$$V_{\partial\Omega_2} = 0. \quad (2.22)$$

The potential of the far boundary is set to 0V in this case. $\partial\Omega_1$ and $\partial\Omega_2$ denote the surface of the model region Ω . There are possible other boundary conditions, like a distributed capacitance approach. Having a split model boundary implies that those conditions can also be mixed in a single model.

2.1.2 Capacitance Evaluation

To calculate the capacitance, the solution for the electric potential V of equation (2.16) is needed. Using Gauss' Theorem

$$Q_{E11} = \int_{\Omega_{E11}} \rho d\Omega = \oint_{\Gamma_{E11}} \vec{\mathbf{D}} \cdot \vec{\mathbf{n}} d\Gamma \quad (2.23)$$

the charge Q_{E11} on electrode *E11* can be expressed as an integral over the surface area Γ_{E11} . The perpendicular vector $\vec{\mathbf{n}}$ is the surface normal of Γ_{E11} , pointing outwards and ρ is the volume charge density.

Using the solution for the scalar potential V_{E11} when electrode *E11* is active and the relation

2 Modeling Capacitive Sensor Effects for Ice Sensors

$$\vec{\mathbf{D}} = \varepsilon_0 \varepsilon_r \vec{\mathbf{E}} = -\varepsilon_0 \varepsilon_r \nabla V \quad (2.24)$$

leads to

$$Q_{E11,E12} = - \oint_{\Gamma_{E12}} \vec{\mathbf{n}} \cdot \varepsilon_0 \varepsilon_r \nabla V_{E11} d\Gamma. \quad (2.25)$$

Equation (2.25) can be used to calculate the total charge $Q_{E11,E12}$ on electrode $E12$ when electrode $E11$ is active. The capacitance C is calculated by

$$C = \frac{Q}{V}, \quad (2.26)$$

where Q is the charge and V the voltage.

The capacitance $C_{E11,E12}$ between electrode $E11$ and electrode $E12$ is then given by

$$C_{E11,E12} = - \frac{1}{V_0} \oint_{\Gamma_{E12}} \vec{\mathbf{n}} \cdot \varepsilon_0 \varepsilon_r \nabla V_{E11} d\Gamma, \quad (2.27)$$

where the voltage V_0 is the potential of the active electrode $E11$ and V_{E11} the solution of the scalar potential.

All influences that are not of interest for the measurement of ice produce an offset in the capacitance. Those influences are assumed to stay constant and can therefore be expressed as the capacitance of the empty sensor C_0 . The relevant information for sensing ice is represented by the change in capacitance. To eliminate the offset, the difference

$$C_{\text{diff};i,j} = C_{i,j} - C_{0;i,j}. \quad (2.28)$$

is evaluated where $C_{0;i,j}$ represents the capacitance between electrodes i and j for an empty sensor.

2.2 Analysis of the Prototype Capacitive Ice Sensor

This section aims to learn properties of an existing capacitive ice sensor. The analysis was conducted by means of a simulation study. This was done to subsequently analyze the sensitivity of the electrodes. Further, measurement experiments in the climatic chamber were used to identify the permittivity of ice.

2.2.1 Electrode Layout

Figure 2.2 depicts the electrode layout of the prototype capacitive ice sensor. A cross-section view is sketched in figure 2.3. It has to be noted that the sketch is not to scale because the thickness of the layers is very thin in comparison to the width of the electrode setup. The sensor features a common transmitter and four receiver electrodes of different size and distances from the transmitter. Electrode three has a unique geometry because it forms a ring around the transmitter and is therefore the closest of the electrodes. On both ends of the sensor, the electrodes are surrounded by a ground layer. The support material of the sensor functions as the insulation layer between the electrodes and the ground plane. For the insulator material a value of $\epsilon_{\text{insulator}} = 5$ is used in the simulations. A support material with a high permittivity would concentrate the electric field in the support material. It could then not be used effectively to sense ice above the sensor.

2.2.2 Capacitive Sensing Circuitry

The capacitive sensing hardware is based on a AD7143 programmable controller for capacitive touch sensors with an integrated calibration logic [16]. It converts capacitances to digital values by measuring the displacement current. Analog to digital conversion of the currents is done by a 16 bit $\Sigma\Delta$ -Analog-to-Digital-Converter ($\Sigma\Delta$ -ADC). It has eight

2 Modeling Capacitive Sensor Effects for Ice Sensors

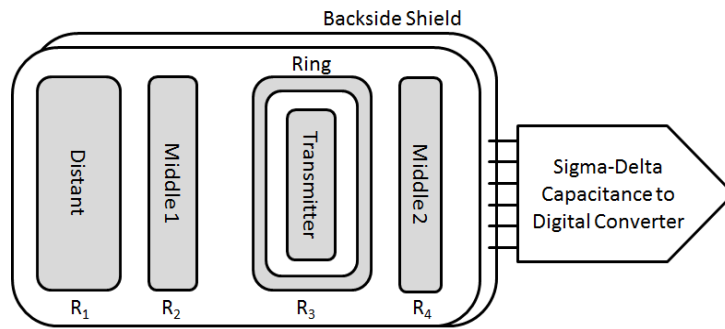


Figure 2.2: Probe and electrode setup of the prototype capacitive ice sensor [12].

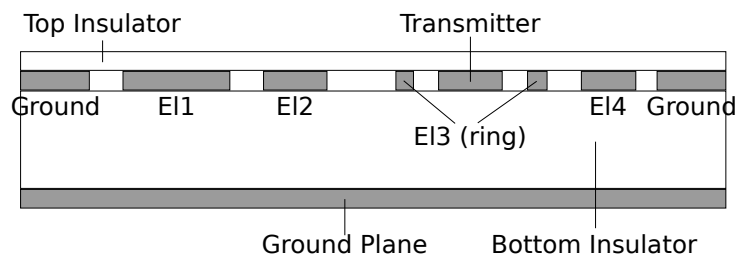


Figure 2.3: Cross-section of the prototype capacitive ice sensor.

2.2 Analysis of the Prototype Capacitive Ice Sensor

inputs which are switched to be measured sequentially. The update rate for all channels is typically 25 ms. An important property to consider for the simulations and for further ice measurements is its transmitter operating frequency, which is 240 kHz. It is of special interest because the permittivity of materials is generally a function of the frequency.

2.2.3 3D-FEM-Simulation Study

To analyze the sensors' behavior in situations which are hard to recreate in experiments, simulations are used. Even ice layers of a certain thickness are needed to assess the sensors' capability to estimate ice thickness. Exactly placed cuboids of ice or water are needed to create a sensitivity map. Both cannot be easily created in the climatic chamber.

The FEM-simulations were made in COMSOL Multiphysics. An electrostatics simulation was chosen to extract the capacitance values. Figure 2.4 shows a section of the 3D-model used in COMSOL. The blue cuboid in the picture represents a raindrop that was placed on the sensor and the red area is the transmitter. The top insulation layer and the far boundary box have been hidden to enable a view of the electrodes.

On the sensor surface, a grid of cuboids, which spans the whole sensor surface with an overlap, has been placed. A rendering of the grid is shown in figure 2.5. The cuboids measure $1\text{ mm} \times 1\text{ mm}$ in width and 0.5 mm in height. Each cuboid can be set to different material properties to represent either air, water, or ice. One cuboid of ice is shown in figure 2.4, where it is colored blue. Every cuboid is set to represent water or ice in turn, while all others are set to represent air. That makes it possible to record each electrodes' individual spatial behavior to water or ice. This method will be used to create a sensitivity map.

Similar to the grid of cuboids, a layer structure was created. By setting the permittivity of the layers to either air or ice, different layer thicknesses could be achieved. Figure 2.6 shows the sensor covered by four active ice layers of 0.5 mm thickness each, resulting in a layer thickness of 2 mm.

2 Modeling Capacitive Sensor Effects for Ice Sensors

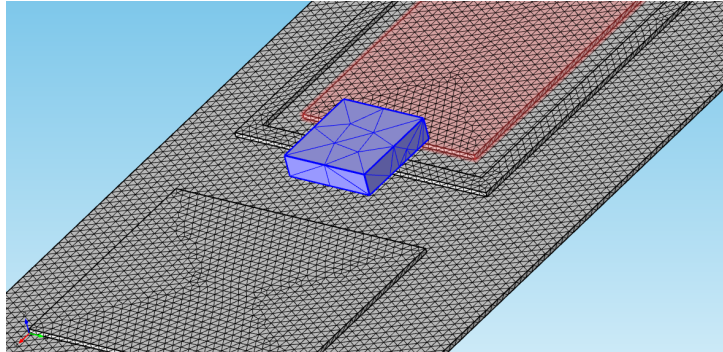


Figure 2.4: 3D-view of a section of the sensor model with one raindrop on the surface.

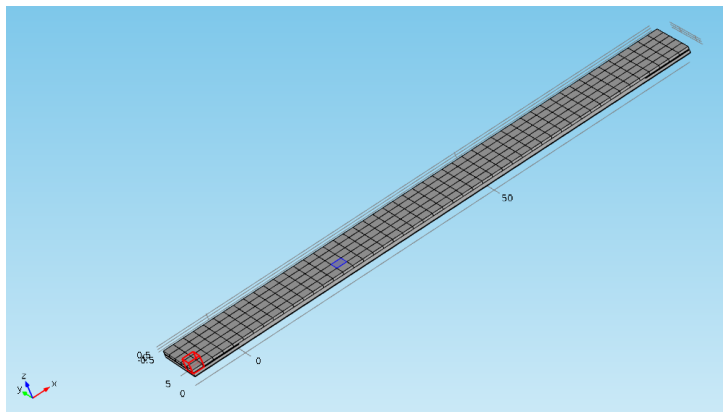


Figure 2.5: 3D-view of the sensor model with the grid of possible cuboid locations.

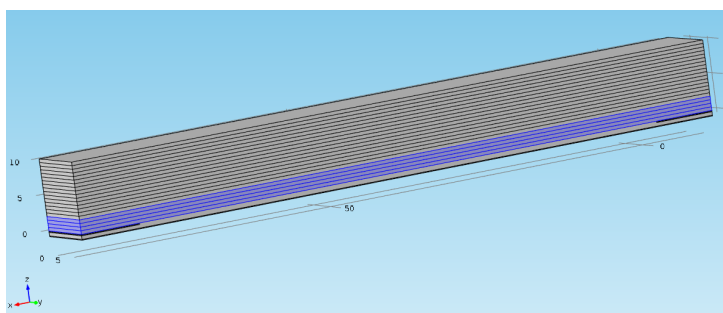


Figure 2.6: 3D-view of the sensor model with an ice layer.

2.2 Analysis of the Prototype Capacitive Ice Sensor

Table 2.1: Relative permittivity values used in the 3D-FEM-simulation study.

Description	Symbol	Value
Relative Permittivity Insulator	$\epsilon_{\text{insulator}}$	5
Relative Permittivity Ice	ϵ_{ice}	3.2
Relative Permittivity Distilled Water, 20 °C	ϵ_{water}	80
Relative Permittivity Air	ϵ_{air}	1.000536
Relative Permittivity Plexiglas	ϵ_{plexi}	3.2

The used permittivity values for ice, water, and air are listed in table 2.1 and are taken from [17] and [18]. Note that the permittivity values for ice will be discussed in detail in section 2.3.

2.2.4 Sensitivity Map Analysis

A spatial sensitivity map of the existing electrode layout of the prototype capacitive ice sensor was created. Its purpose is to show where ice formation produces a spatial change in capacitance and therefore in sensor signal. It can be used to evaluate the electrode layout of the sensor by showing which electrode is sensitive to which climatic scenario.

The sensitivity map can be understood as a quantified representation of the Jacobian matrix

$$J = \frac{dC(\mathbf{x})}{d\mathbf{x}} = \left[\frac{\partial C}{\partial x_1} \quad \dots \quad \frac{\partial C}{\partial x_i} \quad \dots \quad \frac{\partial C}{\partial x_N} \right], \quad (2.29)$$

evaluated for the volume of the cuboids at certain locations. The cuboids' locations are represented by the elements x_i of the vector \mathbf{x} . $C(\mathbf{x})$ is the function that describes the capacitance depending on the location x_i of the cuboid on the sensor. Due to the non-linearity of $C(\mathbf{x})$, the changes in capacitance of individual cuboids cannot be superimposed.

The following sensitivity maps are created with ice cuboids. For each cuboid in the grid that is placed over the sensor the capacitance between each electrode and the common transmitter was computed. This results in

2 Modeling Capacitive Sensor Effects for Ice Sensors

a spatial sensitivity map for each of the electrodes. It has to be noted that the ranges of the values for the different electrodes differ of up to a factor of 300, so they cannot be compared on a single scale.

2.2 Analysis of the Prototype Capacitive Ice Sensor

Electrode 1

Figure 2.7 plots the spatial sensitivity map for the largest electrode 1, which is the farthest away from the common transmitter. The red lines in the plot indicate the positions of the electrodes which correspond to the electrodes in figure 2.2. It shows a high sensitivity on the edges of the electrode and the common transmitter. Ice on the remaining area of the electrode also produces a change in capacitance, albeit smaller. The electrode is not sensitive to ice that is neither directly on the electrode or the transmitter. Electrode 1 produces the overall smallest signals of all the electrodes.

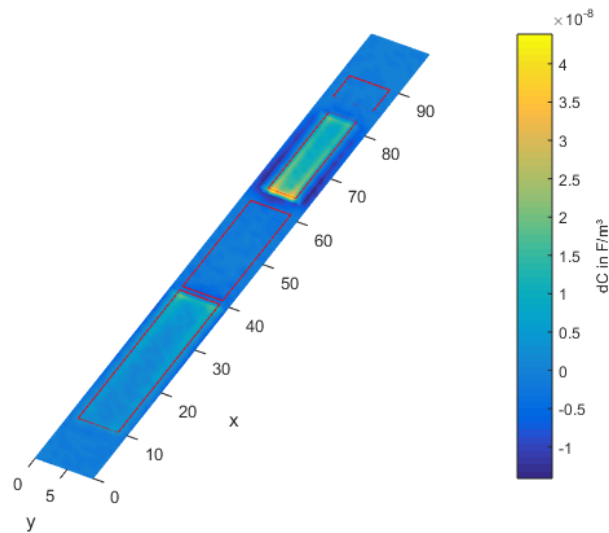


Figure 2.7: Capacitance sensitivity map of electrode 1 for ice.

The negative values in change of capacitance always occur near the common transmitter. They can be explained by the shielding effect of the ground layer beneath the electrodes. The cuboid provides a better path for the electric field towards ground than the air does towards the electrode. This produces a lower capacitance than the capacitance for an empty sensor.

2 Modeling Capacitive Sensor Effects for Ice Sensors

Electrode 2 and Electrode 4

The sensitivity map for electrode 2 is shown in figure 2.8 and that for electrode 4 is depicted in figure 2.9. Those electrodes show a very similar behavior and are therefore discussed together. They are smaller than electrode 1 and closer to the common transmitter. Therefore they produce larger signals compared to electrode 1. Similar to electrode 1, the sensitivities are largest on the edges that face the transmitter as well as the corresponding edge of the transmitter. Contrarily to the far away electrode 1, the sensitivity of the remaining area of the electrodes is small.

Although of different size, the symmetric placement around the common transmitter leads to a nearly identical behavior of electrodes 2 and 4. All those findings lead to the conclusion that a symmetric design of electrodes around the common transmitter is not viable because those electrodes provide the same information.

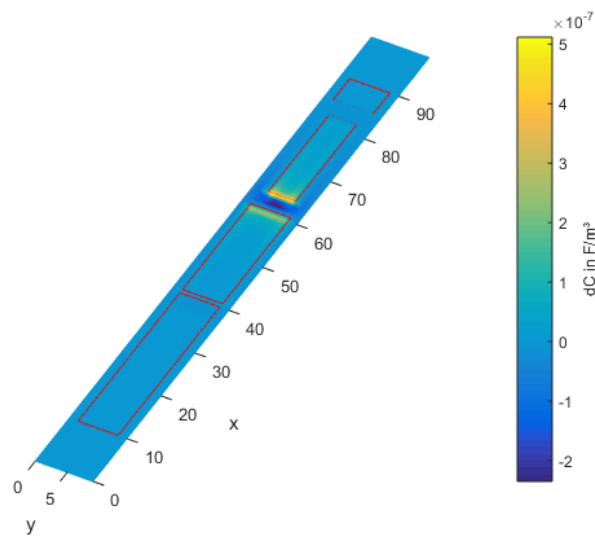


Figure 2.8: Capacitance sensitivity map of electrode 2 for ice.

2.2 Analysis of the Prototype Capacitive Ice Sensor

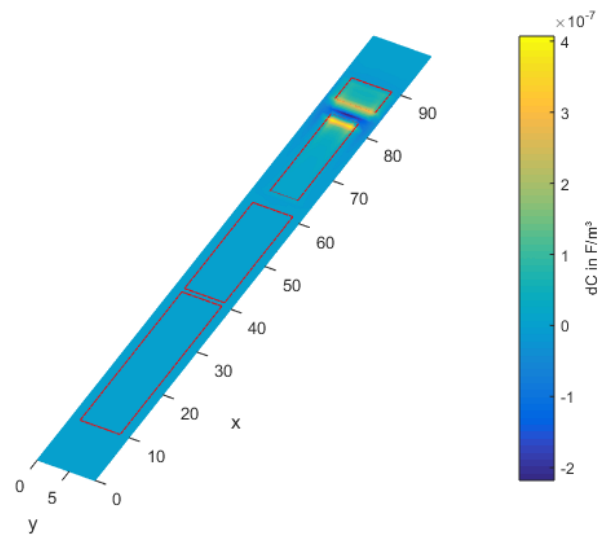


Figure 2.9: Capacitance sensitivity map of electrode 4 for ice.

2 Modeling Capacitive Sensor Effects for Ice Sensors

Electrode 3 (Ring)

Figure 2.10 depicts the sensitivity map for the electrode 3, which is the ring electrode. Its sensitivity values are the largest of all the electrodes but its sensitivity is very local. Ice directly on the ring produces a large change in capacitance while ice that is placed anywhere else does not have any influence.

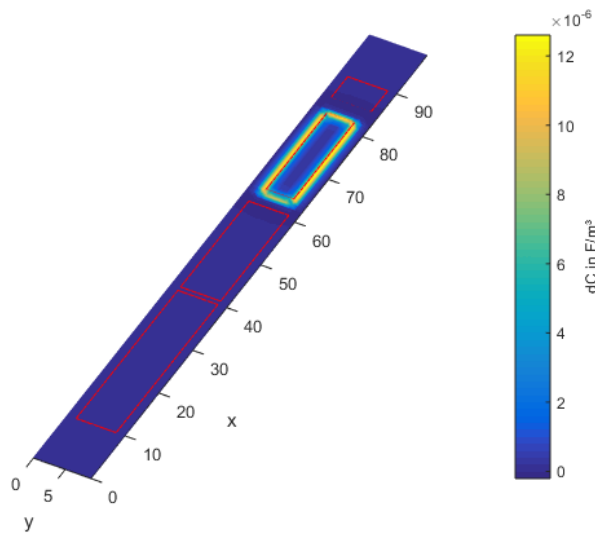


Figure 2.10: Capacitance sensitivity map of electrode 3 (ring) for ice.

The simulations were also done with cuboids of water instead of ice. The results for the electrodes 1, 2, and 4 compared to the results of the simulation with ice cuboids only differ in that all the values are scaled by a factor of 3. They are similar to the pictures of the sensitivity maps for ice and are therefore not depicted. When comparing the results for the ring electrode 3 depicted in figure 2.11, the values increase by a factor of 10, which leads to the conclusion that the narrow structures of the ring electrode are more sensitive to water than to ice compared to the other electrodes.

2.2 Analysis of the Prototype Capacitive Ice Sensor

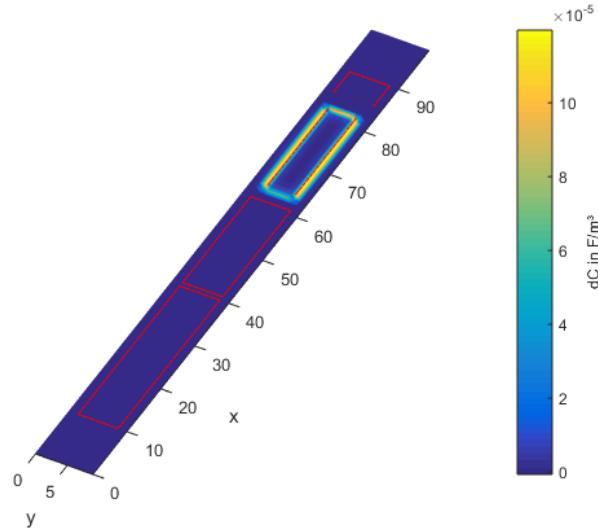


Figure 2.11: Capacitance sensitivity map of electrode 3 (ring) for water.

2.2.5 Ice Layer Thickness Experiment

The behavior of the prototype ice sensor in regard to ice layers of different thickness is of interest. The formation of perfectly even ice layers is complicated to achieve by means of experiments in the climatic chamber. Two approaches to analyze the sensor behavior were used:

- Measurements with a surrogate material.
- Simulation of the sensor for different ice layers.

An experiment with a surrogate material for ice was conducted. Since the permittivity is the main material property important for capacitive sensing, ice can be exchanged for a material with a similar permittivity. Polymethylmethacrylat (PMMA) is a clear plastic with a relative permittivity of

$$\epsilon_{\text{PMMA}} = 3.7, \quad (2.30)$$

which comes close to a typical value for deeply frozen ice of $\epsilon_{\text{ice}} = 3.2$. Plates of 2 mm thickness have been used to represent ice layers.

2 Modeling Capacitive Sensor Effects for Ice Sensors

Figure 2.12 shows the electrodes' behavior for different thicknesses of PMMA.

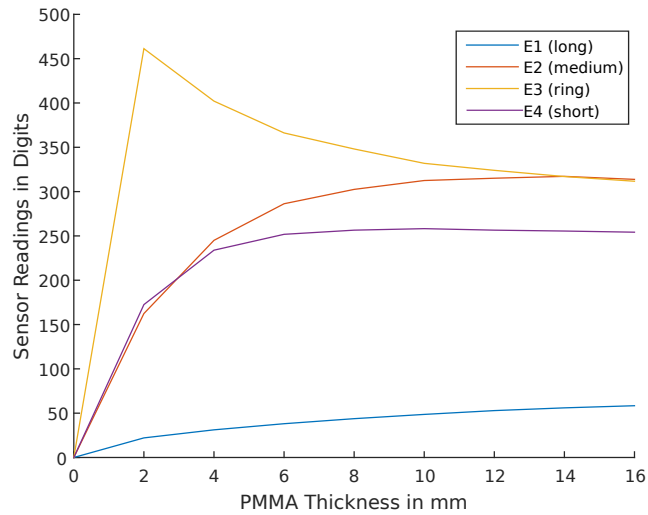


Figure 2.12: Sensor readings for PMMA layers of different thickness.

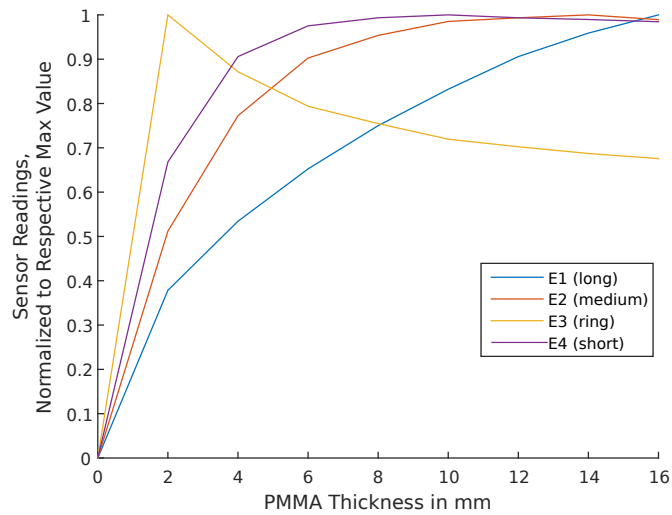


Figure 2.13: Normalized sensor readings for PMMA layers of different thickness.

In a simulation, the sensor was covered with ice layers of different thick-

2.2 Analysis of the Prototype Capacitive Ice Sensor

ness. The simulation used the layer structure discussed in 2.2.3 to represent those ice layers. For each thickness, the capacitance values of all electrodes were computed. The results are plotted in figure 2.14. To better be able to compare the behavior of the simulation in contrast to the PMMA-experiment, the values in figures 2.13 and 2.14 were normalized to each electrodes' respective maximal value. The curves behaving very similar is a sign that the simulation results do indeed match the real sensor.

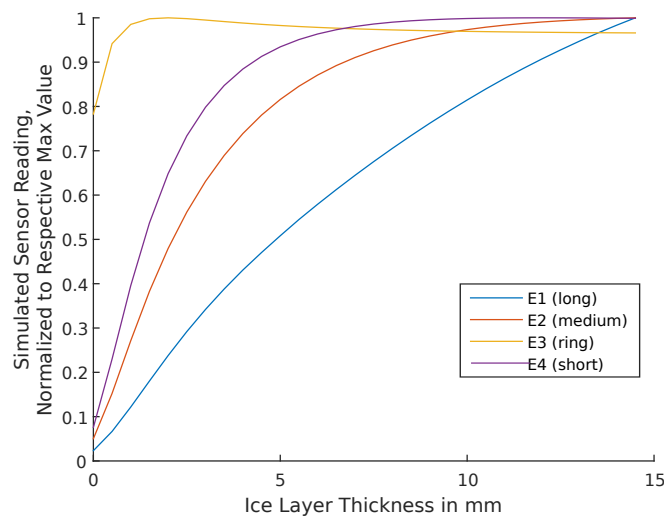


Figure 2.14: Normalized simulated sensor readings for ice layers of different thickness.

Electrode 1

The curve for electrode 1 in figure 2.12 shows that electrode 1 only produces a small sensor reading. It also shows a nearly linear increase in sensor reading over increasing PMMA thickness. Comparing the measured trend depicted in figure 2.13 to the simulated trend in figure 2.14 shows that they match. Electrode 1 can be used to measure ice thicknesses over the whole measurement range without going into saturation. However, its small signal makes it prone to errors from measurement noise.

2 Modeling Capacitive Sensor Effects for Ice Sensors

Electrode 2 and Electrode 4

Electrodes 2 and 4 show a very similar behavior in figure 2.12, like they did in the sensitivity map analysis in section 2.2.4. In the normalized measurements depicted in figure 2.13 this can also be seen. Comparing their normalized trend to the simulation plotted in figure 2.14, the simulated electrodes match the measured behavior. They produce a modest sensor reading but show no linear behavior. For larger ice thicknesses, the sensor reading shows reduced sensitivity. The electrodes cannot be used to distinguish between different thicknesses in this saturation region.

Electrode 3 (Ring)

When comparing the curves for electrode 3, which is the ring electrode, they display the largest deviation between the measurements depicted in figure 2.13 and the simulation depicted in figure 2.14. Since the PMMA layer thickness is increased in steps of 2 mm, the behavior of the measured curve below 2 mm is not representative. Both the measurements and the simulation show that the ring electrode 3 reaches its maximal value at a thin ice layer thickness and is then saturated. It cannot be used to measure ice thickness over a wide range, but only for very thin layers.

2.3 Dielectric Properties of Water and Ice

Water and rain will be modeled by their dielectric properties and dimensions in the later simulations, which will be used for the optimization of the sensor. Therefore, it is important to know the permittivity of ice. Experiments that were conducted in prior studies showed that the permittivity of ice rises under thawing conditions. Since ice will be present in frozen and wet state in a real world sensor application, both scenarios have to be modeled.

2.3 Dielectric Properties of Water and Ice

A coaxial tube probe will be used to analyze the behavior of ice. Since the icing effects in a tube behave differently to those on a planar sensor, the prototype capacitive ice sensor is also used to study wet ice.

In [19] detailed measurements of the permittivity of ice are made in a high frequency band. Different temperatures are also taken into consideration, but the ice is always left to completely freeze. The permittivity for deep-frozen ice averages at $\epsilon_r = 3.2$. The documented change in permittivity is too small to account for the range observed in the measurements. The larger variation in permittivity is therefore not caused by the temperature dependence of ice itself but by another effect.

This effect is suspected to be the content of unfrozen water in ice that is beginning to thaw. Such ice will also be called wet ice in this paper in contrast to deeply frozen, dry ice.

In [20], measurements conducted on ice cores from glaciers are described. Permittivity values between $\epsilon_r = 2.5$ and $\epsilon_r = 3.3$ were observed. Permittivities lower than $\epsilon_r = 3.2$ are caused by trapped air in the ice cores whereas higher values hail from the content of unfrozen water. The experiments were conducted in the temperature range between -25°C to -2°C . It is suspected that wet ice at positive temperatures can reach even higher values due to more unfrozen water.

The conducted measurements in the climatic chamber involved repeated freezing and heating cycles at positive temperatures, so the content of unfrozen water is a likely explanation for the variation. Since the heating cycles also imitate the behavior in nature, the range of occurring values has to be determined to build a reliable simulation scenario thereof.

2.3.1 Coaxial Permittivity Probe

To better study and understand the behavior of the permittivity of ice, a coaxial probe, as depicted in figure 2.15, was built. It consists of a cylindrical tube made of Plexiglas which is sealed on the bottom. The inner electrode is a threaded rod, which is also used to screw the top lid closed. Three more electrodes are mounted on the cylinder on its outside.

2 Modeling Capacitive Sensor Effects for Ice Sensors

Capacitance will be measured between the inner rod electrode and the central large outer electrode. The other two electrodes on the outside will be connected to ground and are used to form a homogenized field between the main electrodes to reduce fringing effects. The exact dimensions of the probe are sketched in figure 2.16.



Figure 2.15: Photo of the coaxial capacitance probe with connection wires.

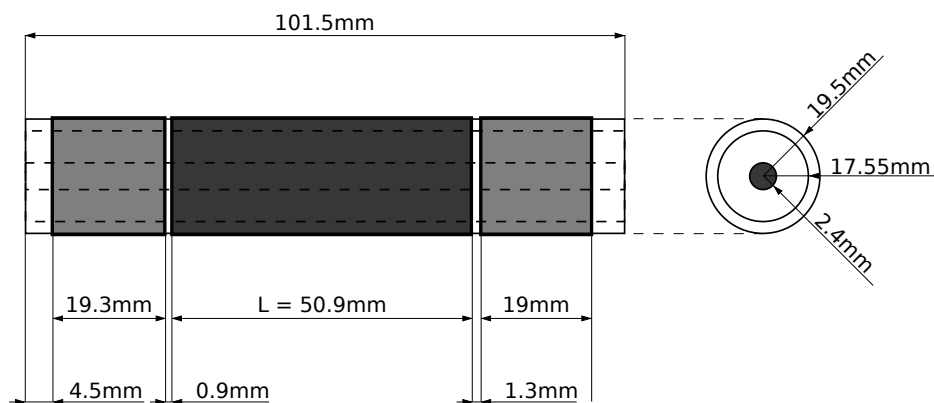


Figure 2.16: Drawing of the coaxial capacitance probe with its dimensions.

To determine the relative permittivity of the material in the probe, the capacitance has to be measured. This was done with an electronic measurement bridge.

The sketch in figure 2.17 shows that the coaxial probe always measures the capacitance of C_1 and C_2 connected in series. Only the capacitance C_1 of

2.3 Dielectric Properties of Water and Ice

the inside of the tube is of interest for determining the permittivity of the material inside. Since the tube's mantle has a certain thickness, there is an added capacitance C_2 between the outer electrode and the inner surface of the tube.

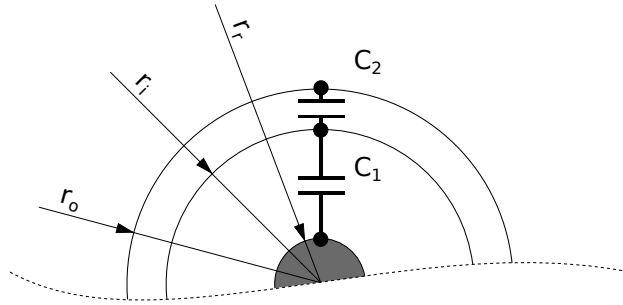


Figure 2.17: Capacitances of the coaxial capacitance probe connected in series.

The capacitance C_2 of the coaxial capacitor formed by the wall of the tube is given by

$$C_2 = \frac{2\pi\epsilon_0\epsilon_{\text{plexi}}}{\ln\left(\frac{r_o}{r_i}\right)} \cdot L, \quad (2.31)$$

where L is the length of the capacitor. The radii r_o and r_i are the outside and inside radii of the probe's tube and $\epsilon_{\text{plexi}} = 3.2$ is the relative permittivity of the tube material [17].

To obtain the capacitance of interest C_1 the constant capacitance C_2 has to be removed from the measured series capacitance C_{series} . The series capacitance C_{series} is given by

$$C_{\text{series}} = \left(\frac{1}{C_1} + \frac{1}{C_2}\right)^{-1}. \quad (2.32)$$

Reforming this formula to express C_1 leads to

$$C_1 = \frac{1}{C_{\text{series}}^{-1} - C_2^{-1}}, \quad (2.33)$$

2 Modeling Capacitive Sensor Effects for Ice Sensors

which can be used to divide the capacitances again. C_{series} is the measured overall capacitance. C_1 denotes the capacitance of interest from the inner electrode rod to the inside surface of the tube. The constant capacitance which has to be removed from the measurements is C_2 .

Since the dimensions stay constant for different measurements, the formula for the capacitance of a cylindrical capacitor could just be reformulated. The relative permittivity is now only a function of the measured capacitance.

The relative permittivity ϵ_r of the material in the coaxial probe is now given by

$$\epsilon_r = \frac{C_1 \cdot \ln\left(\frac{r_i}{r_r}\right)}{L \cdot 2\pi\epsilon_0} \quad (2.34)$$

where C_1 is the capacitance of the inner tube. The radius r_i is the inner radius of the probe tube and r_r is the radius of the rod inside the coaxial probe.

To calibrate the probe, measurements with air and distilled water were made. The known values for those materials from table 2.1 were used.

After calibration, the probe was filled with water and cooled in the climatic chamber at -15°C . The capacitances for the forming ice were measured and figure 2.18 plots the calculated permittivity trend over the time. When no further change in capacitance was observable, the ice was considered fully frozen and dry. The climatic chamber was then heated to 20°C and the ice was left to thaw. A curve composed of the results is plotted in figure 2.19.

The measurements with the cylindrical permittivity probe confirmed the value of relative permittivity for deep-frozen ice at $\epsilon_r = 3.2$. There was no sharp recognizable point in the data curve where a clear transition from dry to wet ice could have happened. The closed construction of the probe does not permit a direct observation of the ice. Therefore, it is not possible to see the transition from water to ice and link it to the measurements. A possible approach for another probe would be an open tank with the electrodes on its plane underside. This setup is also more similar in design

2.3 Dielectric Properties of Water and Ice

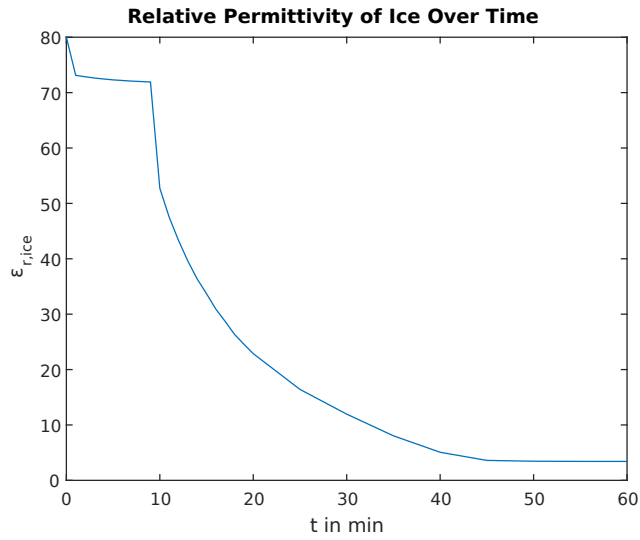


Figure 2.18: Relative permittivity of freezing ice over time at -15°C .

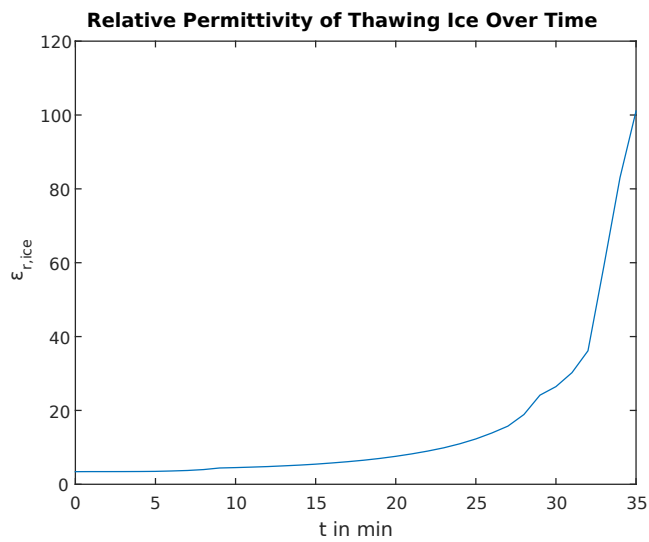


Figure 2.19: Relative permittivity of thawing ice over time at 20°C .

2 Modeling Capacitive Sensor Effects for Ice Sensors

to the ice thickness sensor and would show more of the behavior that is of interest for the design of the sensor.

2.3.2 Ice Properties from Capacitive Measurements

A second approach to analyze the permittivity information of different ice states is to interpret the measurement curves of the prototype capacitive ice sensor. The sensor behavior is simulated for a range of different ice layer thicknesses with different permittivities. The measurements are then compared to the simulation results in a qualitative behavior study. Both the capacitance measurement setup and the simulation do not produce real capacitance values but rather values with an unknown proportional factor. It is consequently best to only rely on the relative behavior of the electrodes.

The permittivity of deeply frozen or dry ice is easily determinable from the cylindrical permittivity probe. Of special interest is the range of the permittivity of ice when it is wet. The plotted curves in figure 2.20 show the measured behavior of the sensor electrodes for a growing layer of deep-frozen ice up to $t_1 = 290$ min. Ice layers are grown by repetitive water mist sprays. All ripples in the signal curves up to t_1 are caused by those sprays. At t_1 the target temperature of the climatic chamber was raised, indicated by the rising chamber temperature $\vartheta_{\text{Chamber}}$. The ice will internally slightly start to thaw as implied by the sudden increase in the sensor reading at $t_2 = 295$ min. This effect is not externally visible to the naked eye and therefore the term wet ice is introduced to refer to ice of that quality.

In figure 2.21, the simulated sensor readings for the electrodes at different ice thicknesses is depicted. Qualitatively, the measured electrode values of electrodes 1, 2 and 4, in relation to each other, behave like those from the simulation. The exception is the behavior of the ring electrode 3. Its simulated values are too large to be depicted in the same scale.

For best comparability, the ice layer in the simulation was chosen to be 5.4 mm, which is the value a previously implemented estimation algorithm for the prototype capacitive ice sensor produced. The picture in

2.3 Dielectric Properties of Water and Ice

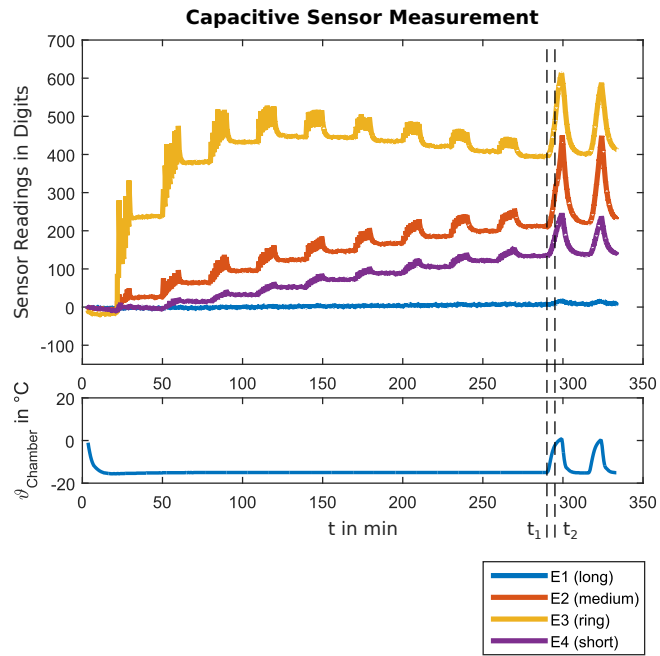


Figure 2.20: Sensor behavior for dry and wet ice.

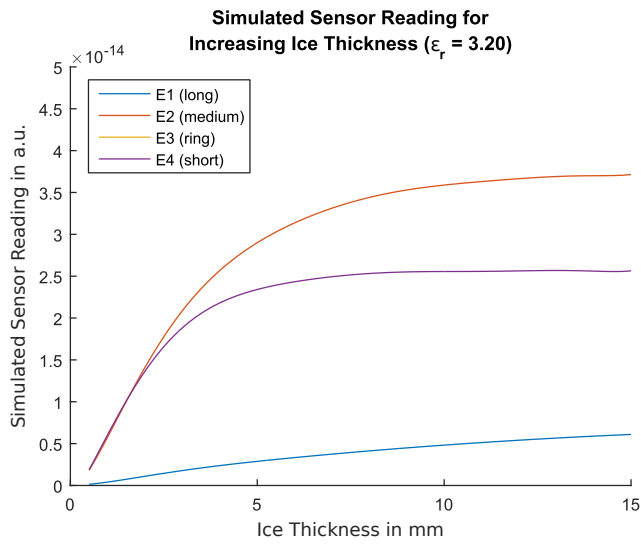


Figure 2.21: Simulated sensor behavior for deep-frozen ice of increasing thickness.

2 Modeling Capacitive Sensor Effects for Ice Sensors

figure 2.22 documents the icing situation right before the heating cycle of the climatic chamber. For best results, the simulations should be done for the actual ice thickness on the sensor, but it is not possible to read an exact value from the picture of the sensor. After heating the chamber, the previously implemented algorithm would show a very different result for the thickness where the pictures show no change in the ice layer thickness or even on the ice's surface. This is an indication that only the permittivity has changed.



Figure 2.22: Picture of the ice layer on the sensor right before the heating cycle.

The measured results of this experiment cannot be directly compared to the simulated results. This is partly because it is not possible to create perfectly homogeneous ice layers of equal thickness on the sensor surface in the climatic chamber with the water mist spray injector. Furthermore, there are noise reduction filters implemented in the prototype. The exact behavior of the used filters is not known and might distort the behavior of the electrodes. Hence, a ratiometric evaluation has to be performed.

Permittivity Estimation for Wet Ice

The permittivity of the ice on the prototype sensor at a certain moment in the measurement depicted in figure 2.20 has to be estimated. Therefore, the sensor readings at those moments are compared to the sensor value at a known reference point. This known reference point is a point where deep-frozen, dry ice can be assumed. For each electrode, a factor is calculated, expressing the increase in sensor value from the deep-frozen state to the wet state. Those factors are then compared to the increase factors of the simulations for different permittivities. When the factors match, the permittivity value for wet ice is found.

The reference point where deep-frozen ice is assumed is at $t_1 = 290$ min after growing and deep-freezing several layers of ice at -18°C . As depicted in the temperature trend, the ice will then be transformed into wet ice by raising the target temperature of the climatic chamber to 20°C . A second reference point is chosen at $t_2 = 295$ min, representing wet ice.

The factor of ice thickness increase f_{inc} is defined by

$$f_{\text{inc}} = \frac{x_{\text{sensor}}(t = t_2)}{x_{\text{sensor}}(t = t_1)}. \quad (2.35)$$

where $x_{\text{sensor}}(t)$ is the sensor reading at the time t . t_1 is the time when the ice is considered deeply frozen. After increasing the temperature, the ice will become wet, which happens at time t_2 . The factors from the measurements are then compared to the factors calculated from the simulation results and used to estimate the relative permittivity of wet ice. The relation of the factors to the relative permittivity taken from the simulation is illustrated in figure 2.23.

All four electrodes provide slightly different results, so the mean value of the relative permittivity for wet ice at $t_2 = 295$ min is calculated to be $\epsilon_r = 4.6$. The largest mean relative permittivity from that measurement was $\epsilon_r = 7.6$ at $t = 299$ min right at the end of the heating cycle before the temperature was lowered again.

2 Modeling Capacitive Sensor Effects for Ice Sensors

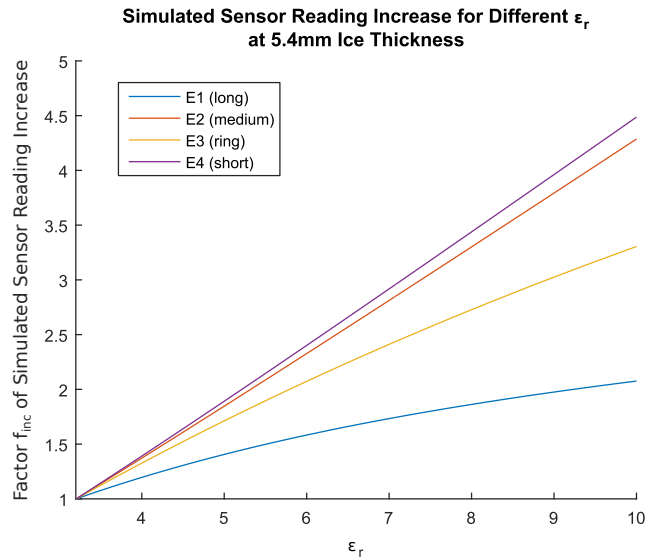


Figure 2.23: Factors of simulated sensor reading increase for different ϵ_r at 5.4 mm ice layer thickness.

2.3.3 Coverage Properties of Ice

The ice patterns which are used to simulate ice behavior in the optimization framework are inspired by the observations made in the climatic chamber experiments as well as from field experiment photos as depicted in 2.22. Especially the case where the ice layer is not even but rather bulging in one area or non-existent in another. Bumps formed by the repeated freezing and heating processes also lead to uneven ice layers. This generally uneven behavior was reflected in the pattern generation process.

2.4 Summary

In this section, all the results from measurements and from studying the prototype capacitive ice sensor are summarized.

2.4 Summary

- The sensitivity map analysis revealed important information about the electrodes. Electrodes with the same distance to the transmitter behave similarly and their information is therefore redundant.
- The electrodes are only sensitive to ice formation directly above the electrode or the common transmitter area. They are especially sensitive on the edges that face each other.
- The ring electrode 3 is more sensitive to water than the other electrodes. Its narrow structures are useful to distinguish between water and ice.
- The experiment that replaces ice layers by surrogate plastic strips showed that the simulation results are comparable to the measured results. This validates the simulation.
- Electrodes show a saturation behavior in which their signal does not increase with increasing ice thickness after a certain point. Saturated electrodes cannot be used to estimate the ice thickness over a certain threshold because of the uncertainty in the saturation region.
- The measurements with the cylindrical permittivity probe confirmed the value of relative permittivity for deep-frozen ice at $\epsilon_r = 3.2$.
- Analyzing the measurements with the prototype capacitive ice sensor led to a range of permittivity values that could occur in wet ice. The highest occurring permittivity value for wet ice was $\epsilon_r = 7.6$.

3 Sensor Simulation Framework

This chapter deals with the creation of a sensor simulation and optimization framework, which provides a general platform for all further investigations. The sensor model geometry can be constructed, simulated and subsequently optimized with the help of the framework. It incorporates the knowledge about capacitive sensing and the behavior of ice from chapter 2.

Figure 3.1 shows the general proposed form of an ice sensor, together with its measurement electronics and an evaluation algorithm. Together, these components can be considered a measurement system. A method for creating and simulating sensors for different ice scenarios is discussed in this chapter. Reconstruction algorithms which are needed to assess the performance of a sensor will be discussed in the separate chapter 4.

The flow chart in figure 3.2 was created to illustrate the work-flow of an optimization study and to visualize the concepts. All the necessary steps are discussed in detail in the following sections.

To simulate different geometric sensor setups, a generic sensor model with variable parameters is used. It describes the general form of a capacitive ice sensor and is used to create a specific sensor for the simulations. All the components of the generic model are discussed.

As can be seen in figure 3.1, the proposed general sensor design has a constant cross-section. Since this makes it well suited for 2D-simulation, this approach is chosen over the more complex 3D-simulation.

For the evaluation of the performance of a sensor, a way to simulate ice and rain behavior is needed. Perfectly even ice accretion with constant permittivity does rarely occur outside of a simulation. Due to the random nature of ice and rain, a method to simulate the sensor with stochastically

3 Sensor Simulation Framework

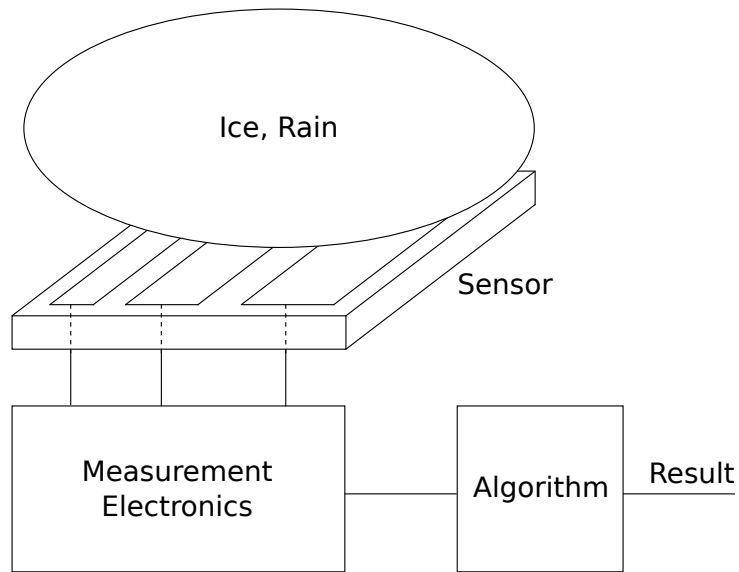


Figure 3.1: Measurement system of the ice sensor.

generated scenarios is discussed. A single randomized representation of an ice or rain scenario is called a pattern. With the pattern generator, a generation algorithm for those scenarios is introduced. The pattern prototypes which describe the general form of a scenario are presented.

Each sensor design has to be simulated for numerous different patterns to evaluate its behavior under many possible conditions. The optimization process also requires repeated evaluation during the iterations of the sensor designs. To reduce the simulation time, material mapping, a method for fast simulation of different patterns, is discussed.

3.1 Generic Sensor Simulation Model

At the core of the optimization process is the electrostatic simulation of the sensor. The simulation result is used to calculate the capacitances between the electrodes. A generic sensor model with variable parameters is needed to create different sensors for the optimization process. The model is sketched in figure 3.3, but note that the drawing is not to scale.

3.1 Generic Sensor Simulation Model

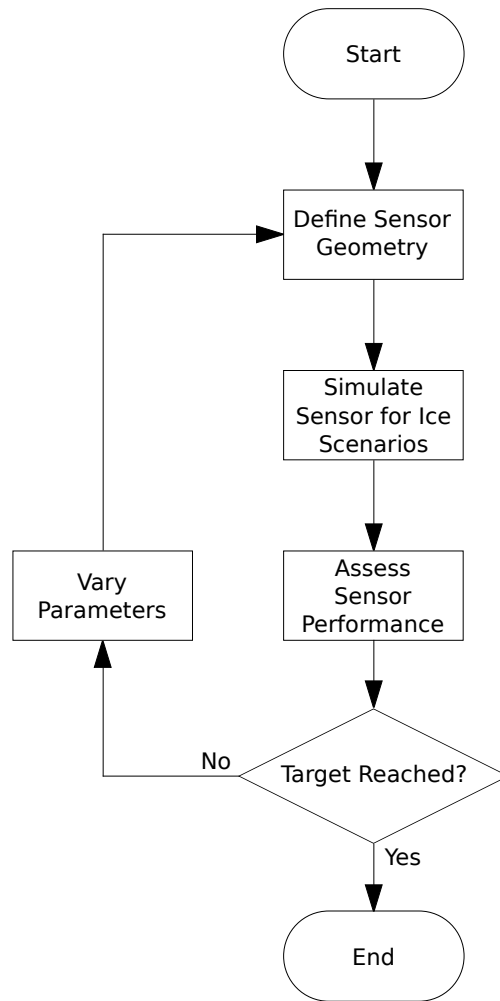


Figure 3.2: Flowchart of the optimization process.

3 Sensor Simulation Framework

This is because in reality the structures are very thin compared to the overall size of the sensor.

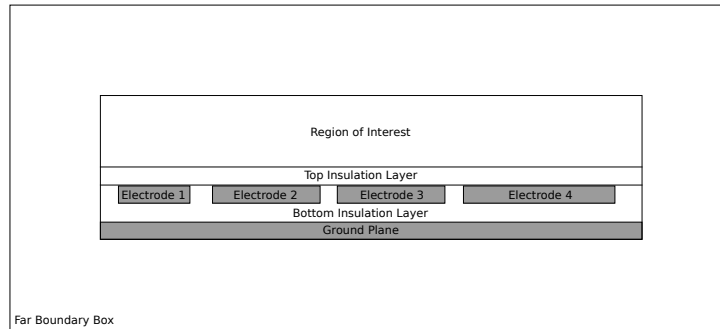


Figure 3.3: Illustration of the generic sensor model for four electrodes.

The geometric parameters of the model are variable to adapt to different electrode setups. Other parameters like the number of electrodes and the permittivities of the insulation material are changeable to the needs of the individual sensor.

The different parts included in the sensor model are:

- Electrodes - used for capacitive ice sensing.
- Region of interest ROI - area where ice or rain on the sensor is modeled.
- Ground plane - shields the sensing electrodes.
- Insulation layers - protect the sensing electrodes and insulate them from each other.
- Far boundary box - used to define the potential far away from the sensor.

An illustration of the model in figure 3.3 shows the arrangement of the different regions of the model. Each part is described in detail in the following subsections.

3.1.1 Electrodes

With respect to the sensor behavior, the electrode geometry has the largest influence. The geometry parameters describe the electrode setup of a

3.1 Generic Sensor Simulation Model

sensor and will be the main variables in the optimization process. For each electrode, the geometry parameters consist of its width and its distance to the next electrode. The thickness is a common parameter for all electrodes in the model and is typically not used as a variable for the optimization process.

In figure 3.4, a narrow electrode is visible in white, surrounded by the green and blue insulation layers. Since the electrodes are usually very thin, they can only be seen in a zoomed view of the FEM-mesh. The ground plane is also visible in white beneath the insulation layer. All metal regions are excluded from the simulation because there is no electric field within a conductor.

At the start of the optimization process, the number of electrodes is chosen. Restrictions for individual minimal and maximal widths, as well as the maximal overall width of the sensor, can be set.

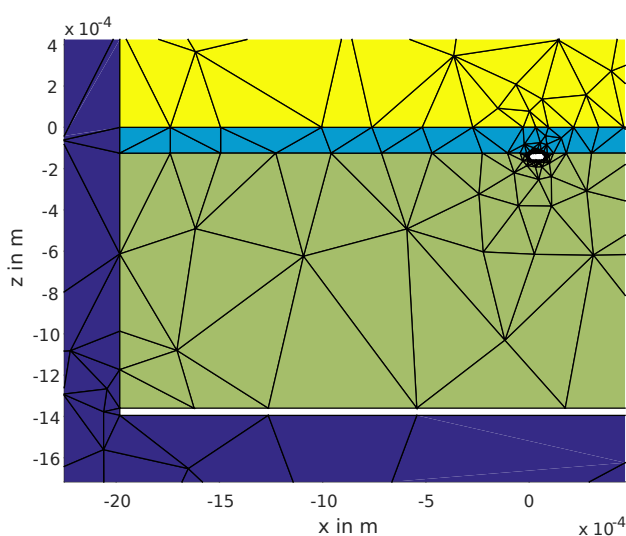


Figure 3.4: Mesh of the sensor, zoomed to an electrode.

The corners of the electrodes are rounded, as can be seen in figure 3.5. Sharp corners produce local singularities in the calculation of the charge distribution which results in numerical errors. To counteract this, the corners of the electrodes are designed in a rounded manner. Additional

3 Sensor Simulation Framework

triangles are needed to mesh the round corners, so they come at the cost of more elements in the calculation [21].

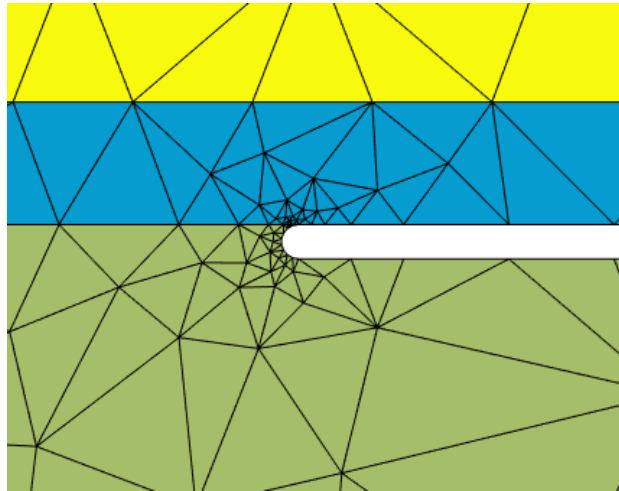


Figure 3.5: Rounded corners of an electrode in the mesh.

3.1.2 Region of Interest

The area right above the top insulation layer is where the rain and ice scenario will be formed in the simulation. It is referred to as the region of interest (ROI) because it is used to represent the physical quantity of interest. The ROI is depicted in figure 3.6, where it is the area consisting of small yellow triangles above the sensor. The width of the ROI always spans the whole sensor surface and its height corresponds to the maximum ice thickness parameter.

Rain and ice are described through their permittivity and distribution in the ROI. Each scenario of rain or ice is computed to assign a specific permittivity to every triangle of the mesh inside this area. To achieve a fine spatial resolution, the maximum size of the mesh triangles inside the ROI has to be specified. The triangles have to be significantly smaller than the ice and rain scenario structures.

3.1 Generic Sensor Simulation Model

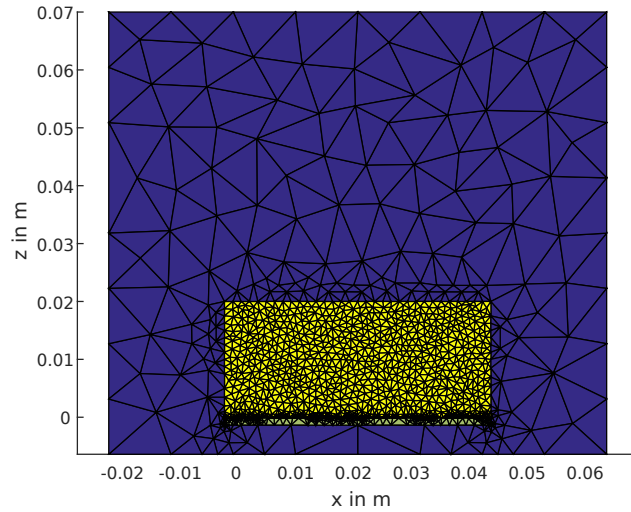


Figure 3.6: Mesh of a sensor and simulation region.

Additional information on pattern creation and the mapping of the patterns to the ROI can be found in the subsection 3.2.1.

3.1.3 Ground Plane

The ground plane, illustrated in figure 3.3, constitutes the bottom side of the sensor. It is used to shield the electrodes from influences from below so that they only sense changes due to ice and rain above them. It always spans the whole sensor width and its only parameter is its thickness.

3.1.4 Insulation Layers

The insulation layers separate the electrodes from each other and from the ground plane. They also protect the electrodes from outside influences. In the generic model depicted in figure 3.3, the insulation is split in a bottom and a top layer. Those layers could consist of different materials, described by their respective thicknesses and permittivities.

3 Sensor Simulation Framework

3.1.5 Far Boundary Box

A boundary box is used to describe the behavior of the potential V on the boundary of the modeling region of the sensor. It is placed around the sensor, as is depicted in figure 3.3. The boundary will always influence the sensor in some way. To reduce this influence, the boundary is placed far away from the sensor.

A larger boundary box will also result in more triangles in the mesh, so a trade-off between simulation accuracy and simulation complexity has to be made. The mesh generator automatically increases the triangle size towards the far boundary, so in practice there are not too many additional triangle nodes.

A Dirichlet boundary condition is used, setting the potential V of the far boundary to 0 V.

3.2 Rain and Ice Pattern Generation

A method to generate random ice and rain scenarios is needed to replicate the natural behavior of ice and rain in a simulation. Figure 3.7 shows a generic sensor with an example of an ice scenario in the ROI. This behavior is imitated with a pattern generator, where a single pattern represents one specific ice or rain scenario. A pattern describes the placement of rain drops or the ice growth on the sensor surface.

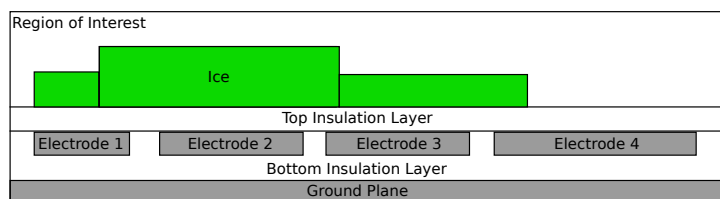


Figure 3.7: Ice scenario on a generic sensor.

Pattern prototypes are used to provide the general form and behavior of a scenario. They include randomized parameters to create different random

3.2 Rain and Ice Pattern Generation

patterns corresponding to the prototype formulation. The generator uses the pattern prototypes to produce any number of randomized ice or rain patterns. Which pattern prototypes are used in an optimization of a sensor is summarized in a pattern statistic. A pattern statistic describes the range of real world situations the sensor has to deal with. It includes the probability for each pattern prototype to occur in a simulation and produce one of its random patterns.

3.2.1 Material Mapping

Each sensor has to be simulated for numerous different patterns to evaluate its behavior under many possible conditions. Material mapping of ice and rain patterns to the ROI of the sensor model is used to achieve a faster simulation. Figure 3.8 shows the process of mapping a pattern to the ROI, after which it represents the ice or rain scenario of the used pattern.

The approach of modeling different ice situations as part of the sensor model geometry would require the generation of a new mesh for each pattern. Generation of the mesh from the geometry parameters of the sensor model is computationally expensive. To avoid the need to re-mesh the geometry, an area of variable permittivity, is introduced to the model.

Every triangle in the mesh of the model has a list of properties assigned to it. In case of the electrostatic FEM-simulation, each triangle can represent an area of material defined by its permittivity value. The geometrical center of each triangle is used to identify the triangles' positions on the pattern and assign its permittivity correspondingly. To calculate the coordinates of the center O from the three triangle nodes A , B , and C the formulae

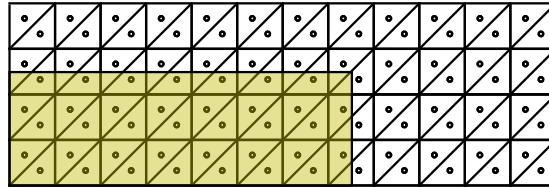
$$O_x = \frac{A_x + B_x + C_x}{3} \quad (3.1)$$

and

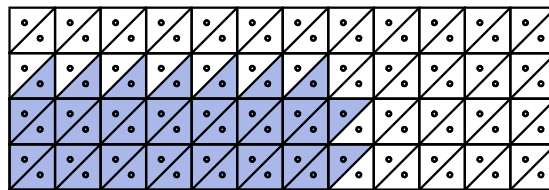
$$O_y = \frac{A_y + B_y + C_y}{3} \quad (3.2)$$

3 Sensor Simulation Framework


Region of Interest



Region of Interest



 Ice Pattern

 Ice Pattern applied to the Region of Interest

- Center of Gravity of a Triangle

Figure 3.8: Mapping of a pattern onto the Region of Interest.

3.2 Rain and Ice Pattern Generation

are used for the x and y coordinate respectively. An alternate approach would be to assign the average permittivity of the triangles corners to each triangle, but using the center of gravity is faster.

3.2.2 Pattern Prototypes

Pattern prototypes refer to a set of fundamental ice and rain scenarios. Figure 3.9 depicts the prototype for a simple block of ice. Several prototypes are defined in order to provide realistic scenarios for natural ice accretion. To achieve a generation of different patterns, some key parameters of the prototypes are randomized.

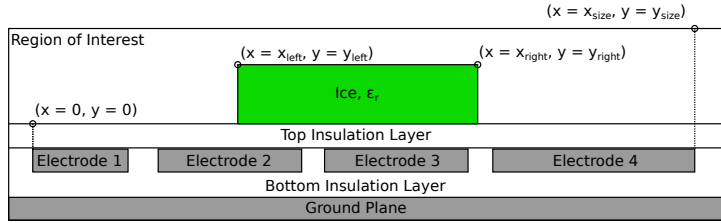


Figure 3.9: Pattern prototype for a single block of ice.

Each prototype describes its patterns through blocks of material, like the ice block sketched in figure 3.9. Its geometry, location and permittivity is described by the variables shown in the drawing. The variables of one block are summarized in a vector \mathbf{p}_i which has the form

$$\mathbf{p}_i = \begin{bmatrix} x_{\text{left}} \\ x_{\text{right}} \\ y_{\text{left}} \\ y_{\text{right}} \\ \epsilon_r \end{bmatrix}^T, \quad (3.3)$$

where x_{left} and y_{left} are the coordinates of the top left corner of each block. For the top right corner of each block the coordinates are given by x_{right} and y_{right} . All coordinates are relative to the point indicated by $x = 0, y = 0$ in figure 3.9. The permittivity of the block is denoted by ϵ_r .

3 Sensor Simulation Framework

For more complex ice patterns or for raindrops, a single block is not enough. A matrix \mathbf{P} with an arbitrary number of rows \mathbf{p}_i is used to represent a prototype with multiple blocks. The pattern generator will then use this matrix \mathbf{P} to create a single specific pattern from the prototype. Due to the randomness in the placement of blocks, it is possible for them to overlap. Blocks with a larger thickness precede thinner blocks. By randomizing the variables of each block, the prototype can be used to generate a variety of different patterns that share a fundamental form, but for instance vary in thickness.

The coordinates are usually expressions including the parameters for the maximal ice layer thickness y_{size} and the total sensor width x_{size} . Additionally, the permittivity values for deep-frozen $\varepsilon_{\text{ice,frozen}}$ and wet ice $\varepsilon_{\text{ice,wet}}$ are used. A random variable r_i is used in those formulae so that each prototype can create different randomized versions of its pattern. The random variable r_i follows a uniform distribution described by

$$r_i \propto \mathcal{U}(0,1). \quad (3.4)$$

The number of vectors \mathbf{p}_i can also be random to, for instance, create a variable number of rain drops on the sensor surface. Since some patterns use multiple random variables r_i , the index i is used to indicate which represent the same value inside a vector \mathbf{p}_i .

3.2.3 Pattern Statistic

A pattern statistic is used to describe which pattern prototypes will be used for the simulation. It lists the prototypes to use, together with their probability to be selected and produce a pattern. Through the use of this list of probabilities, it is possible to describe a wide range of scenarios each with an arbitrary number of pattern prototypes. A typical pattern statistic looks like:

- 50 % - Pattern Prototype A
- 30 % - Pattern Prototype B
- 20 % - Pattern Prototype C.

3.2 Rain and Ice Pattern Generation

It can be made up of any number of pattern prototypes, but the probabilities have to sum up to 100%. Which scenarios were used to conduct the design studies and their pattern statistic will be described in each design study in chapter 5.

3.2.4 Rain Patterns

All pattern prototypes for rain share the same square raindrop size of 1 mm by 1 mm. The patterns differ in the number of drops which are distributed over the sensor surface, simulating light or heavy rain.

3 Sensor Simulation Framework

Four Raindrops

Different pattern prototypes for a fixed number of raindrops could be implemented. As an example shown in figure 3.10, a pattern with four randomly placed raindrops is depicted. It is represented by a matrix \mathbf{P} with four rows

$$\mathbf{p}_i = \begin{bmatrix} x_{\text{left}} \\ x_{\text{right}} \\ y_{\text{left}} \\ y_{\text{right}} \\ \varepsilon_r \end{bmatrix}^T = \begin{bmatrix} (x_{\text{size}} - 1 \text{ mm}) \cdot r_1 \\ (x_{\text{size}} - 1 \text{ mm}) \cdot r_1 + 1 \text{ mm} \\ 1 \text{ mm} \\ 1 \text{ mm} \\ \varepsilon_{\text{water}} \end{bmatrix}^T, \quad (3.5)$$

where $\varepsilon_{\text{water}} = 80$ is the permittivity of water. The drops are 1 mm by 1 mm in dimension and can be placed anywhere on the sensor surface. This is done by using the randomized value r_1 which follows a uniform distribution between 0 and 1.

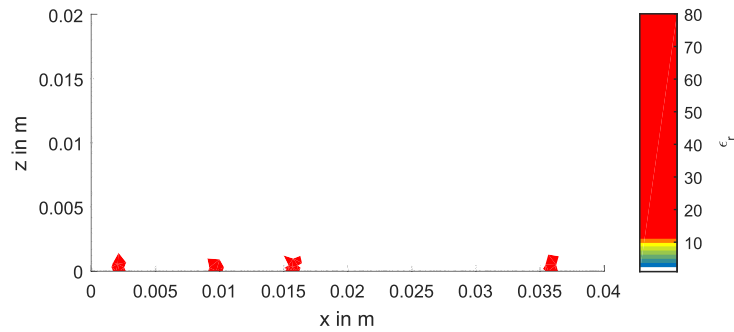


Figure 3.10: Example of a pattern “Four Raindrops”.

3.2 Rain and Ice Pattern Generation

Variable Number of Raindrops

To create patterns that could represent a wide variety of rain events, a prototype with a variable number of raindrops was created. One pattern created this way is depicted in figure 3.11. The maximum count of drops n

$$n = \left\lceil \frac{x_{\text{size}}}{1 \text{ mm}} \cdot r_1 \right\rceil \quad (3.6)$$

is dictated by the total width of the sensor x_{size} so that potentially the whole surface could be covered in water. It is created by a matrix \mathbf{P} with the n rows

$$\mathbf{p}_i = \begin{bmatrix} x_{\text{left}} \\ x_{\text{right}} \\ y_{\text{left}} \\ y_{\text{right}} \\ \varepsilon_r \end{bmatrix}^T = \begin{bmatrix} (x_{\text{size}} - 1 \text{ mm}) \cdot r_1 \\ (x_{\text{size}} - 1 \text{ mm}) \cdot r_1 + 1 \text{ mm} \\ 1 \text{ mm} \\ 1 \text{ mm} \\ \varepsilon_{\text{water}} \end{bmatrix}^T. \quad (3.7)$$

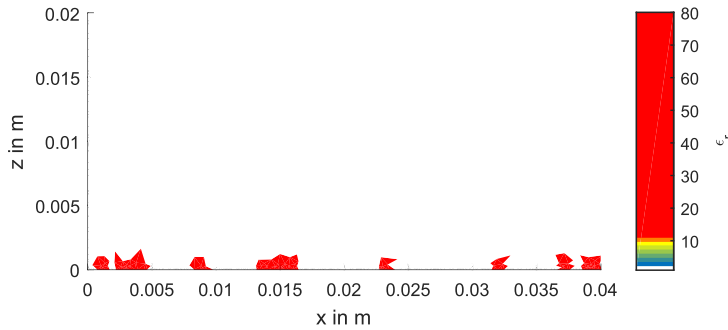


Figure 3.11: Example of a pattern “Variable Number of Raindrops”.

3 Sensor Simulation Framework

Thin Film of Water of Variable Thickness

A unique pattern prototype for a thin film of water of variable thickness was created and can be seen in figure 3.12. It is represented by the vector \mathbf{p}_1 which is

$$\mathbf{p}_1 = \begin{bmatrix} x_{\text{left}} \\ x_{\text{right}} \\ y_{\text{left}} \\ y_{\text{right}} \\ \varepsilon_r \end{bmatrix}^T = \begin{bmatrix} 0 \\ x_{\text{size}} \\ 100 \mu\text{m} \cdot r_1 \\ 100 \mu\text{m} \cdot r_1 \\ \varepsilon_{\text{water}} \end{bmatrix}^T, \quad (3.8)$$

and creates a film of water up to $100 \mu\text{m}$ thick that covers the whole sensor. It is used to simulate the situation when the whole sensor is wet right before the water freezes and ice forms.

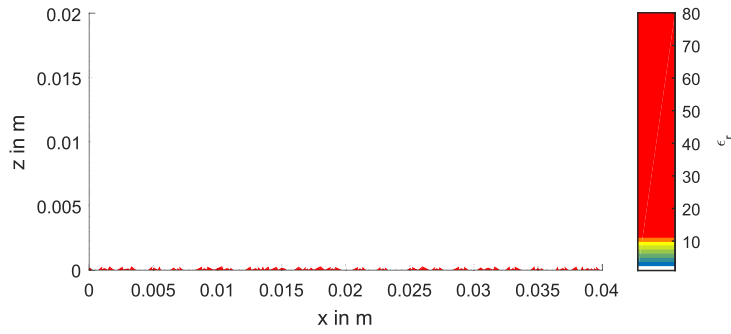


Figure 3.12: Example of a pattern “Thin Film of Water of Variable Thickness”.

3.2.5 Ice Patterns

Ice pattern prototypes incorporate the observations made in the climatic chamber experiments as well as experiments in the field. Results from the study of dielectric properties of ice made in section 2.3 are used. The core characteristic is that ice has a wide range of permittivity values due to its content of unfrozen water.

The pattern prototypes created to represent ice come in two variants each. One to represent deep-frozen ice with a constant permittivity of $\epsilon_{\text{ice,frozen}} = 3.2$ and one to represent ice in different states of wetness. Wet ice is characterized by randomized permittivity values in the range from $\epsilon_{\text{ice,frozen}} = 3.2$ to $\epsilon_{\text{ice,wet}} = 7.6$.

To assess the performance of an estimation algorithm, the real ice thickness of a pattern has to be known to compare it against the estimate. The ice thickness of a rectangular block is specified by y_{left} . In case of a pattern with multiple blocks and uneven coverage, the average thickness over the sensor surface is computed.

3 Sensor Simulation Framework

Deep-Frozen Ice Layer of Varying Thickness Covering the Whole Sensor

An example of a deep-frozen ice layer of randomly varying thickness is depicted in figure 3.13. The pattern prototype is described by the vector

$$\mathbf{p}_1 = \begin{bmatrix} x_{\text{left}} \\ x_{\text{right}} \\ y_{\text{left}} \\ y_{\text{right}} \\ \varepsilon_r \end{bmatrix}^T = \begin{bmatrix} 0 \\ x_{\text{size}} \\ y_{\text{size}} \cdot r_1 \\ y_{\text{size}} \cdot r_1 \\ \varepsilon_{\text{ice,frozen}} \end{bmatrix}^T, \quad (3.9)$$

where the only random parameter is the thickness. This pattern always covers the whole sensor evenly with deep-frozen ice.

The effects of the material mapping can be seen in figure 3.13. Since there is no new mesh created for each pattern, the edges will appear ragged. The smallest chunk of material with a dedicated permittivity is a triangle from the ROI. A finer discretization can be used to achieve smoother edges.

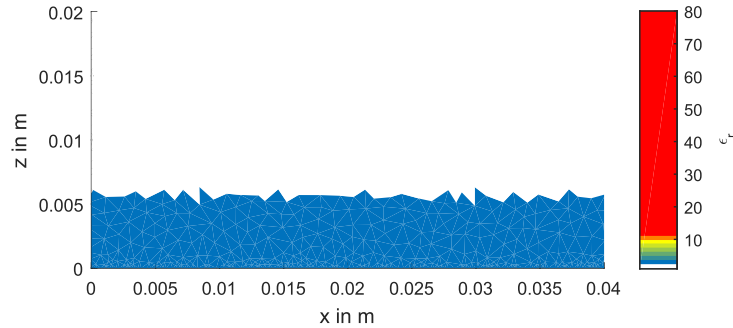


Figure 3.13: Example of a pattern “Deep-Frozen Ice Layer of Varying Thickness Covering the Whole Sensor”.

3.2 Rain and Ice Pattern Generation

Wet Ice Layer of Varying Thickness Covering the Whole Sensor

There is also a variant of the previous pattern with variable permittivity to represent all kinds of wet ice, which is illustrated in figure 3.14. It is represented by the vector

$$\mathbf{p}_1 = \begin{bmatrix} x_{\text{left}} \\ x_{\text{right}} \\ y_{\text{left}} \\ y_{\text{right}} \\ \epsilon_r \end{bmatrix}^T = \begin{bmatrix} 0 \\ x_{\text{size}} \\ y_{\text{size}} \cdot r_1 \\ y_{\text{size}} \cdot r_1 \\ \epsilon_{\text{ice,frozen}} + (\epsilon_{\text{ice,wet}} - \epsilon_{\text{ice,frozen}}) \cdot r_2 \end{bmatrix}^T. \quad (3.10)$$

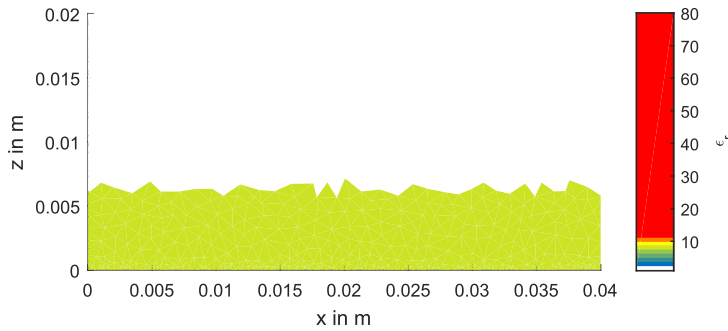


Figure 3.14: Example of a pattern “Wet Ice Layer of Varying Thickness Covering the Whole Sensor”.

3 Sensor Simulation Framework

Deep-Frozen Ice of Varying Thickness Covering Half the Sensor

Taking the observations into account, it became obvious that ice will not always cover the sensor's surface evenly throughout. Those scenarios are represented by the following pattern prototypes. The first, which is depicted in figure 3.15, will cover only half of the sensor area with deep-frozen ice. It is described by vector

$$\mathbf{p}_1 = \begin{bmatrix} x_{\text{left}} \\ x_{\text{right}} \\ y_{\text{left}} \\ y_{\text{right}} \\ \varepsilon_r \end{bmatrix}^T = \begin{bmatrix} \frac{x_{\text{size}}}{2} \cdot r_1 \\ \frac{x_{\text{size}}}{2} \cdot r_1 + \frac{x_{\text{size}}}{2} \\ y_{\text{size}} \cdot r_2 \\ y_{\text{size}} \cdot r_2 \\ \varepsilon_{\text{ice,frozen}} \end{bmatrix}^T, \quad (3.11)$$

where r_1 and r_2 are two different randomized values.

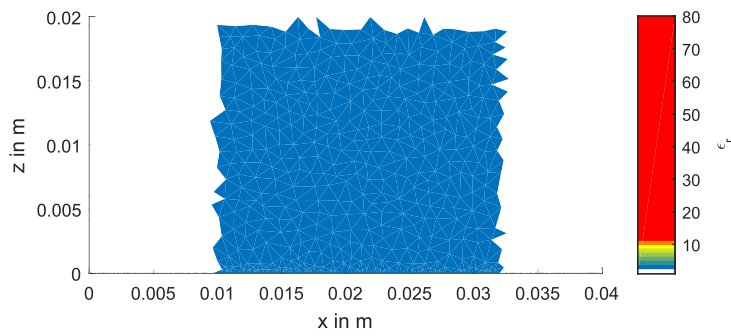


Figure 3.15: Example of a pattern “Deep-Frozen Ice of Varying Thickness Covering Half the Sensor”.

3.2 Rain and Ice Pattern Generation

Wet Ice of Varying Thickness Covering Half the Sensor

The pattern depicted in figure 3.16 is very similar to the previous pattern but with wet ice instead. It will cover only half of the sensor area with various states of wet ice. It is described by the vector

$$\mathbf{p}_1 = \begin{bmatrix} x_{\text{left}} \\ x_{\text{right}} \\ y_{\text{left}} \\ y_{\text{right}} \\ \varepsilon_r \end{bmatrix}^T = \begin{bmatrix} \frac{x_{\text{size}}}{2} \cdot r_1 \\ \frac{x_{\text{size}}}{2} \cdot r_1 + \frac{x_{\text{size}}}{2} \\ y_{\text{size}} \cdot r_2 \\ y_{\text{size}} \cdot r_2 \\ \varepsilon_{\text{ice,frozen}} + (\varepsilon_{\text{ice,wet}} - \varepsilon_{\text{ice,frozen}}) \cdot r_3 \end{bmatrix}^T, \quad (3.12)$$

where r_1 and r_2 are two different randomized values.

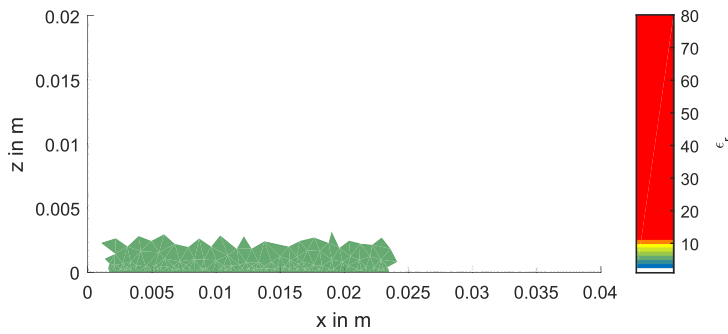


Figure 3.16: Example of a pattern “Wet Ice of Varying Thickness Covering Half the Sensor”.

3 Sensor Simulation Framework

Wet Ice of Varying Thickness Unevenly Covering the Sensor

A similar pattern prototype covers the sensor in up to four ice patches of a quarter of the sensor's width each. Slightly wet ice with $\varepsilon_r = 4$ is used. This scenario is depicted by the pattern in figure 3.17. It is represented by a matrix \mathbf{P} with a randomized number of rows n calculated by

$$n = \lceil 4 \cdot r_1 \rceil, \quad (3.13)$$

where each row is given by

$$\mathbf{p}_i = \begin{bmatrix} x_{\text{left}} \\ x_{\text{right}} \\ y_{\text{left}} \\ y_{\text{right}} \\ \varepsilon_r \end{bmatrix}^T = \begin{bmatrix} \frac{3x_{\text{size}}}{4} \cdot r_1 \\ \frac{3x_{\text{size}}}{4} \cdot r_1 + \frac{x_{\text{size}}}{4} \\ y_{\text{size}} \cdot r_2 \\ y_{\text{size}} \cdot r_2 \\ 4 \end{bmatrix}^T. \quad (3.14)$$

There could be between 1 and 4 rows, each corresponding to one block of ice. The random variables for the thickness of the blocks are evaluated separately, creating an uneven surface. Those partly covering patterns could represent an uneven icing process due to wind or portions of ice falling off from the sensor.

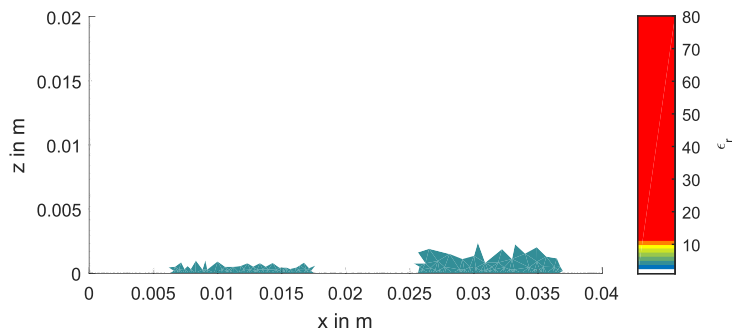


Figure 3.17: Example of a pattern "Wet Ice of Varying Thickness Unevenly Covering the Sensor".

Thin, Wet Ice Layer of Varying Thickness Covering the Whole Sensor

The last type of pattern represents thin layers of ice either frozen or still wet and freezing. Those are used in the optimization of the ice detector to simulate the initially forming ice layer. A depiction of this ice layer can be seen in figure 3.18. It is created by the vector

$$\mathbf{p}_1 = \begin{bmatrix} x_{\text{left}} \\ x_{\text{right}} \\ y_{\text{left}} \\ y_{\text{right}} \\ \varepsilon_r \end{bmatrix}^T = \begin{bmatrix} 0 \\ x_{\text{size}} \\ 1 \text{ mm} \cdot r_1 \\ 1 \text{ mm} \cdot r_1 \\ \varepsilon_{\text{ice,frozen}} + (\varepsilon_{\text{ice,wet}} - \varepsilon_{\text{ice,frozen}}) \cdot r_2 \end{bmatrix}^T, \quad (3.15)$$

and covers the whole sensor surface with a layer of variable thickness of up to 1 mm. The permittivity is variable in the range of wet ice. The ice detector is used to distinguish between water and freshly formed ice. It is important to use thin layers because ice will start forming that way.

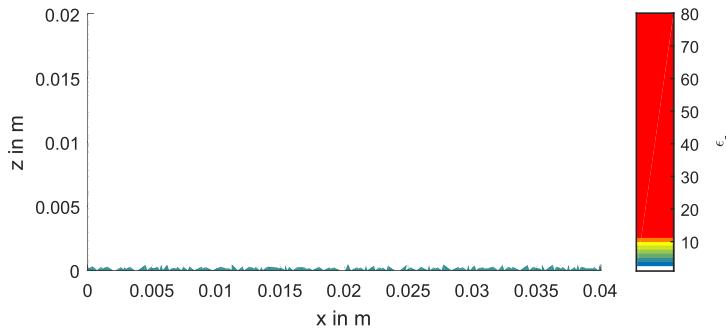


Figure 3.18: Example of a pattern “Thin, Wet Ice Layer of Varying Thickness Covering the Whole Sensor”.

3.3 Complete Simulation Process

In the complete process of simulating a sensor, its behavior is evaluated for numerous different scenarios. All the necessary steps for a complete simulation process of a sensor are:

1. Sensor Creation
 - Geometry parameters.
 - Electrode configuration.
2. Pre-processing
 - Create mesh.
 - Set up FEM-simulation.
 - Simulate sensor under empty conditions.
3. Simulation
 - Simulate the sensor for defined patterns.
 - Post-processing of capacitances.

A new sensor is created by choosing the parameters for the generic sensor model. The parts of the sensor model are described in section 3.1. For this specific sensor, a mesh is created by a mesh generator provided by [22] and the FEM-simulation is prepared.

The simulation itself is done with the help of a framework developed at the EMT [15]. It supports fast 2D-simulations with different material parameters. To evaluate numerous different ice or rain scenarios, the sensor is simulated for every pattern created for this simulation process. Patterns are applied to the ROI by the material mapping process described in section 3.2.1.

From the simulations' results, the capacitances of interest are computed. This step is detailed in the following subsection 3.3.1.

After processing the capacitances, they are handed to the objective function to be evaluated. The specific steps of an optimization process are discussed in the following section 3.4.

3.3.1 Post-Processing of Capacitance

Some post-processing of the capacitance values is needed. Every new sensor is also once simulated under empty conditions, which provides the capacitances C_0 . To further observe only the change in capacitance due to different patterns on the sensor, the capacitance C_0 is subtracted from all subsequently computed capacitance values.

One electrode is usually the common transmitter due to the sensing electronics described in 2.2.2. The position of the common transmitter in the order of the electrodes is set at the beginning of the complete optimization process. All capacitance values of the other electrodes in respect to the transmitter are calculated. It is also possible to compute the inter-electrode capacitances.

The ice detector will use a capacitive finger structure. It consists of repeated small electrodes which are alternately interconnected to form a single large capacitor with two electrodes. The interconnection is not existent in the simulations but rather is achieved by computation of the capacitance values.

3.4 Complete Optimization Process

The complete iterative optimization process utilizes all the parts of the framework to optimize a sensor. An evaluation of the performance of a sensor is needed to compare different design iterations to each other.

This evaluation is done by means of an objective function, which computes a single value as a measure of the sensor's performance. Criteria for what exactly constitutes a good sensor have to be incorporated into this function. Each design approach will generally need its own specifically formulated objective function. Since this is an important part of the optimization process, the distinct chapter 4 is dedicated to the design of objective functions.

3 Sensor Simulation Framework

All the steps of the complete optimization process are illustrated in figure 3.2 and outlined here:

1. Start
 - Define general electrode configuration.
 - Define general parameter limits.
 - Define sensor performance threshold or maximum number of iterations limit.
2. Define Sensor Geometry
 - New geometry parameters for the complete simulation process, described in section 3.3.
3. Simulate Sensor with Scenarios
 - Complete simulation process, described in section 3.3.
4. Assess Sensor Performance
 - Objective function, described in chapter 4.
5. Target Reached?
 - Compare sensor performance to threshold.
 - Compare number of iterations to the limit.
6. Vary Parameters
 - Vary parameters of the sensor geometry.
7. End
 - Optimal parameters of the sensor geometry found.

At the start of a complete optimization process, the general parameters of the sensor are defined. This includes the number of electrodes and all limitations as well as the position of the common transmitter electrode.

Random starting parameters for the geometry are chosen for the first iteration of the sensor. The sensor is subject to the complete simulation process, as described in section 3.3. It simulates the sensor behavior for a number of different scenarios. The performance of the sensor iteration is then evaluated by the objective function. Designing different objective functions is discussed in chapter 4.

Comparison of the objective function values and the variation of the geometry parameters are done by an optimization algorithm. For all optimization results of the design studies in chapter 5, the Differential Evolution algorithm was used [23]. The algorithm will try to minimize the given objective function by varying the geometry parameters.

The end of the complete optimization process is reached when the sensor performance value is smaller than a defined threshold. If the threshold cannot be reached, the process stops after a defined number of iterations. Either way, the process provides geometry parameters that are better suited for sensing the scenario on the sensor than others. They can be considered optimal in that regard.

3.5 Summary

In this section, the most important points of the sensor simulation framework are summarized.

- A generic sensor simulation model is needed to create a wide variety of sensors. They can be defined by the parameters of the generic model. Due to the design of the model, all sensors share the same general form.
- Rain and ice show a random behavior in nature. To imitate that situation in a simulation, randomly generated scenarios, represented by patterns, are used. To evaluate the sensor performance, numerous simulations with different patterns are needed in a complete simulation process.
- Fast simulation of different patterns is provided by the method of material mapping. It is not necessary to generate a new mesh of the model for each ice or rain scenario.
- Optimization is done in an iterative process. Objective functions are needed to evaluate the performance of a sensor iteration. An optimization algorithm compares the different results and varies the geometry parameters to create new sensor designs.

4 Design of Optimized Sensors

Designing appropriate objective functions is a key part of the iterative optimization process. The objective function, also known as cost function, is used to evaluate a sensor design by assigning a single value to it. This value represents the performance of the sensor.

The sensor simulation framework will create a new sensor iteration by varying some input parameters. Simulations with different ice or rain patterns are then made with the new sensor, computing the electrodes' capacitance values to the common transmitter. The objective function now has to evaluate the sensor with the help of the simulated capacitances. For comparison, the pattern information like the true thickness of an ice pattern is used.

The challenge is to first understand which properties of the sensor are important to achieve a certain task. Two important tasks of the ice sensor are:

- Ice detection,
- Ice amount sensing,

where the sensing of the ice amount is done by estimating the thickness of the ice layer on the sensor. The performance of a sensor is then expressed as a single value which has to be optimized. However, the sensor is only optimal with respect to the formulated objective function.

Ice detection is used to detect the presence of ice or rain on the sensor and then distinguish between the two situations. Only when the presence of ice is detected, an attempt to estimate its thickness is viable. The information whether ice is present is also important for monitoring the danger potential on critical surfaces.

4 Design of Optimized Sensors

When the presence of ice has been detected, the ice amount sensor can be utilized to estimate the thickness of the ice. This information is useful to further judge the danger potential and coordinate countermeasures.

The sensing electrode setup together with the measurement electronics and the detection or estimation algorithm can be considered a measurement system. It is also possible to include the algorithm in the objective function and then optimize the whole system rather than just the electrode setup.

In the simulations of the sensor behavior, randomized patterns of ice or rain are used. Therefore, statistical evaluations of the simulation results have to be performed.

4.1 Ice Detector Design

An ice detector is used to detect the presence of anything other than air and to distinguish between ice and rain. After introducing a basic detector, methods to evaluate its performance are discussed. Methods using a binary classification test can be applied when only the two cases ice and rain are considered.

A detector operating on a single capacitance C uses the thresholds T_{ice} and T_{rain} to distinguish between the three scenarios

$$\hat{x}(x) = \begin{cases} \text{nothing (empty sensor)} & \text{if } C(x) < T_{\text{ice}} \\ \text{negative (ice)} & \text{if } T_{\text{ice}} < C(x) < T_{\text{rain}} \\ \text{positive (rain)} & \text{if } C(x) > T_{\text{rain}} \end{cases} \quad (4.1)$$

where \hat{x} is the detector result and x the information about the actual situation on the detector. The thresholds are sketched in figure 4.1, where T_{ice} is the threshold that determines whether the detector is considered empty. When the capacitance C reaches the threshold T_{rain} , the scenario on the sensor is considered to be rain.

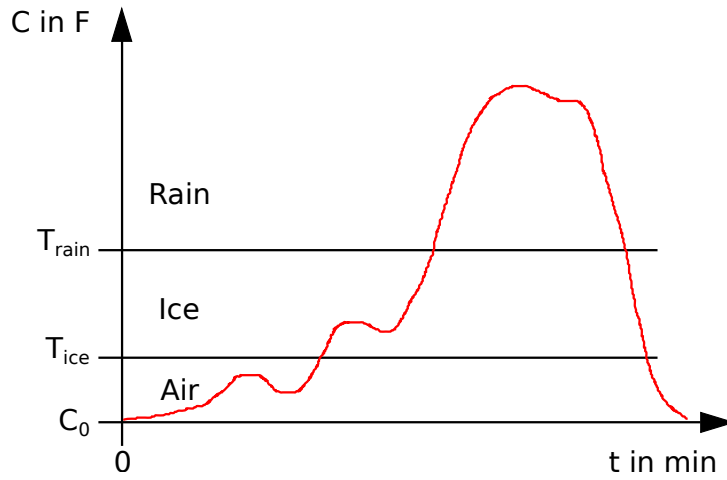


Figure 4.1: Thresholds of the ice detector.

The further design of the objective function will only consider the two scenarios rain and ice, so that methods of binary classification tests can be applied. This simplifies the detector to

$$\hat{x}(x) = \begin{cases} \text{negative (ice)} & \text{if } C(x) < T_{\text{rain}} \\ \text{positive (rain)} & \text{if } C(x) > T_{\text{rain}}. \end{cases} \quad (4.2)$$

In order to evaluate the performance two methods are discussed:

- The receiver operating characteristic ROC, which is a visual aid for finding the optimal threshold.
- Youden's index, which expresses the detector performance as a value.

Youden's index is more useful in the context of an optimization process because it is expressed as a value that can be maximized.

The results from analyzing the prototype capacitive ice sensor in section 2.2 revealed that the close electrode design of the ring electrode was useful in detecting water. Consequently, the ice detector was designed as a series of close and narrow electrodes interconnected alternately. This design, known as finger structures, is basically a single capacitor consisting of

4 Design of Optimized Sensors

several capacitors connected in parallel. This structure is used to boost the overall signal strength of the parameter which is to be measured [9].

4.1.1 Binary Classification

The binary classification test performance measures use the true positive rate (TPR) and the false positive rate (FPR) to evaluate a binary detector. To calculate them, the detector has to be simulated with different ice and rain patterns. The detection function is then applied to the simulated capacitances C . All detector results \hat{x} from one complete simulation process are represented by the vector $\hat{\mathbf{x}}$. The detection results $\hat{\mathbf{x}}$ are then compared to the actual ice or rain situation expressed by the vector \mathbf{x} . They are classified using the table 4.1.

Table 4.1: Classification of detection events.

\hat{x} (detected) \ x (actually)	positive	negative
positive	true positive	false positive
negative	false negative	true negative

The TPR and the FPR are defined by

$$\begin{aligned} \text{TPR} &= P(\text{detected positive} | \text{actually positive}) \\ &= \frac{\Sigma_{\text{truepositive}}}{\Sigma_{\text{actuallypositive}}} \end{aligned} \quad (4.3)$$

and

$$\begin{aligned} \text{FPR} &= P(\text{detected positive} | \text{actually negative}) \\ &= \frac{\Sigma_{\text{falsepositive}}}{\Sigma_{\text{actuallynegative}}}, \end{aligned} \quad (4.4)$$

where the values Σ_i indicate the number of how often event i has occurred.

By evaluating the detector performance for different threshold values, the best threshold for the detector can be found.

Receiver Operating Characteristic

The receiver operating characteristic (ROC) is a visual aid to find the optimal threshold parameter for a detector [24]. A generic ROC-curve for a binary detector is shown in figure 4.2. Each threshold values' performance is represented by one point on the blue ROC curve. In the ice detector, the threshold is used to distinguish between rain and ice.

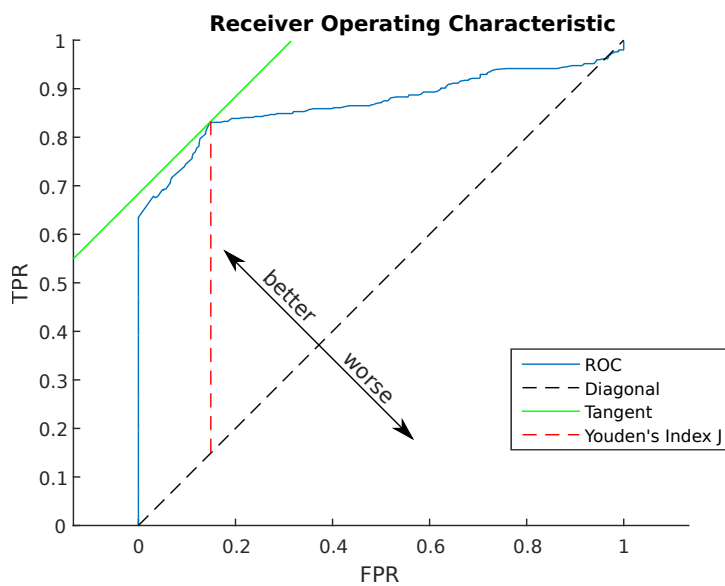


Figure 4.2: Receiver Operating Characteristic.

Each detector design is simulated with a scenario of ice and rain patterns and the detected events \hat{x} are classified, as in table 4.1, and counted.

To create the ROC-curve, the TPR is plotted against the FPR. This is done for all the different threshold values which are to be compared. The best threshold value is then determined by the threshold in the top left of the ROC-curve. Note that the value of the best threshold cannot actually be read from the plot. A ROC-curve near the diagonal would indicate a random process because the TPR and FPR are nearly equal for each threshold value.

4 Design of Optimized Sensors

Youden's Index

The graphical evaluation of the detector performance is impractical for an optimization process. A more formal approach than the ROI is needed to design an objective function. Youden's index is such a formal approach, expressing the detector performance as a value between -1 and 1 . Since it is closely related to the ROC it can also be plotted in the same figure 4.2. By optimizing for the largest Youden's index, the best detector setup and its best threshold can be found [25].

Youden's index J of a detector for a given threshold is calculated as follows

$$J = \text{TPR} + \text{TNR} - 1, \quad (4.5)$$

where the true negative rate (TNR) is needed. The TNR can be expressed as $1 - \text{FPR}$ which simplifies the formula for Youden's index to

$$J = \text{TPR} - \text{FPR}, \quad (4.6)$$

which combines the same two parameters used in the creation of the ROC-curve.

Youden's index expresses the requirement of a large TPR combined with a small FPR. This means a high chance of detecting actual rain as rain and a low chance of falsely detecting ice as rain. A Youden's index J near 0 would indicate a random process where the detection results do not correspond to the actual situation, similar to a ROC-curve near the diagonal.

4.1.2 Objective Function

The introduction of Youden's index J leads to the formulation of the objective function as

4.2 Linear Ice Sensor Design with One Capacitance

$$\mathbf{v}_{\text{optimal}} = \arg \min(-J(\mathbf{v})). \quad (4.7)$$

The vector \mathbf{v} represents the variables of the optimization problem which express the electrode geometry. $\mathbf{v}_{\text{optimal}}$ are the optimized values for those parameters. A larger Youden's index J indicates that the detector is better at distinguishing between the two cases. Since the used optimization algorithm will always try to minimize the objective function, $-J$ is used.

4.1.3 Computational Steps

This subsection describes the necessary computational steps to simulate and evaluate an ice detector. Those steps will be repeated by the optimization algorithm until an optimal solution is found.

1. Create a specific electrode geometry for the sensor.
2. Simulate the sensor with numerous ice and rain patterns corresponding to the pattern statistic.
3. Find the threshold with the maximum Youden's index J .
4. Evaluate and return the value of the objective function.

4.2 Linear Ice Sensor Design with One Capacitance

After ice has been detected on a critical surface, its mass is also of interest. For a critical surface of constant area, the thickness is a measure of the ice mass. Therefore, a sensor has to be optimized for the estimation of ice layer thickness.

The ice sensor is a measurement system as illustrated in figure 3.1. A simple reconstruction algorithm can be desired for a lightweight and power saving implementation. In general a sensor with a linear behavior is preferable. For an electrode setup with only one capacitance and ideal linear behavior a very simple estimation algorithm like

4 Design of Optimized Sensors

$$\hat{x} = k \cdot C(x, \mathbf{v}) \quad (4.8)$$

is required, where \hat{x} is the estimated ice thickness. The measured capacitance C depends on the real ice thickness x , as well as the geometry parameters \mathbf{v} of the electrodes. The factor k is the proportional factor used to reconstruct the ice thickness x from the measured capacitance C . This reconstruction assumes that the capacitance C increases linearly with the ice thickness x on the sensor.

As the analysis made in section 2.2 showed, this is not generally the case. Nevertheless, the electrode geometry of a single capacitor sensor can be optimized for its best possible linear behavior. The methods can be expanded to a multiple capacitance approach and are therefore explained at the example of a single capacitance sensor first.

For a newly created sensor, the value for the proportionality factor k has to be determined. The sensor is simulated with different ice patterns and the capacitances C are calculated. All capacitances from the complete simulation process are represented by the vector \mathbf{C} . A single capacitance sensor generally does not show an ideal linear behavior. The best fit to all the simulated capacitances \mathbf{C} has to be calculated by solving the overdetermined systems of equations

$$\mathbf{x} = \mathbf{C}(\mathbf{x}) \cdot k \quad (4.9)$$

for the factor k . This least squares problem can be solved by

$$k = \mathbf{C}(\mathbf{x})^+ \cdot \mathbf{x} \quad (4.10)$$

where \mathbf{C}^+ is the pseudo-inverse of \mathbf{C} .

The vector \mathbf{x} holds the true thicknesses of all the patterns the sensor has been simulated with.

To optimize the behavior of a single capacitance sensor for the best linear behavior, a measure for its performance is needed. The error

4.2 Linear Ice Sensor Design with One Capacitance

$$e_x = \hat{x} - x \quad (4.11)$$

for a single estimation is given by the difference of the estimated ice thickness \hat{x} and the real ice thickness x . Inserting equation (4.8) results in

$$e_x = k \cdot C(x, \mathbf{v}) - x, \quad (4.12)$$

expressing the error e_x depending on the simulated capacitance C .

The mean squared error (MSE)

$$\text{MSE} = E\{e_x^2\}, \quad (4.13)$$

is calculated by evaluating the expectation of the error e_x for all the patterns in the complete simulation process. The MSE is then used as the optimization criterion. Since the MSE can also be expressed as

$$\text{MSE} = \text{bias}_x^2 + \sigma_x^2, \quad (4.14)$$

it represents a combination of the bias and variance σ_x^2 values. The square root of the variance σ_x^2 is the standard deviation σ_x . This makes the MSE a more useful measure in contrast to the error e_x for the optimization.

The bias is given by

$$\text{bias}_x = E\{e_x\} \quad (4.15)$$

and the variance by

$$\sigma_x^2 = E\{(e_x - \text{bias}_x)^2\}. \quad (4.16)$$

4 Design of Optimized Sensors

4.2.1 Objective Function

An optimal sensor has a minimal MSE which is achieved by varying the sensor's geometry represented by \mathbf{v} . It is the objective to find the most appropriate values for the geometry $\mathbf{v}_{\text{optimal}}$. The objective function can therefore be expressed as

$$\mathbf{v}_{\text{optimal}} = \arg \min(\text{MSE}(\mathbf{v})). \quad (4.17)$$

4.2.2 Computational Steps

This subsection describes the necessary computational steps to simulate and evaluate a linear ice sensor with one capacitance. Those steps will be repeated by the optimization algorithm until an optimal solution is found.

1. Create a specific electrode geometry for the sensor.
2. Simulate the sensor with numerous ice patterns corresponding to the pattern statistic.
3. Determine the factor k for the linear thickness estimator.
4. Use the linear thickness estimator to compute thickness estimates \hat{x} .
5. Evaluate and return the value of the objective function.

4.3 Linear Ice Sensor Design with Multiple Capacitances

As the analysis made in section 2.2 showed, the capacitances of the ice sensor do not behave linearly for increasing ice thicknesses. Most of the analyzed electrodes, though, show a nearly linear behavior over a certain range of ice thickness. This makes it necessary to combine the measurements of multiple electrodes to cover the whole measurement range. Figure 4.3 illustrates the behavior of three capacitances for even ice layers of different thicknesses and the combined behavior. The approach

4.3 Linear Ice Sensor Design with Multiple Capacitances

to find an optimal linear design for a sensor with multiple electrodes is very similar to the optimization of a single capacitance sensor. The same methods described in section 4.2 are used and expanded.

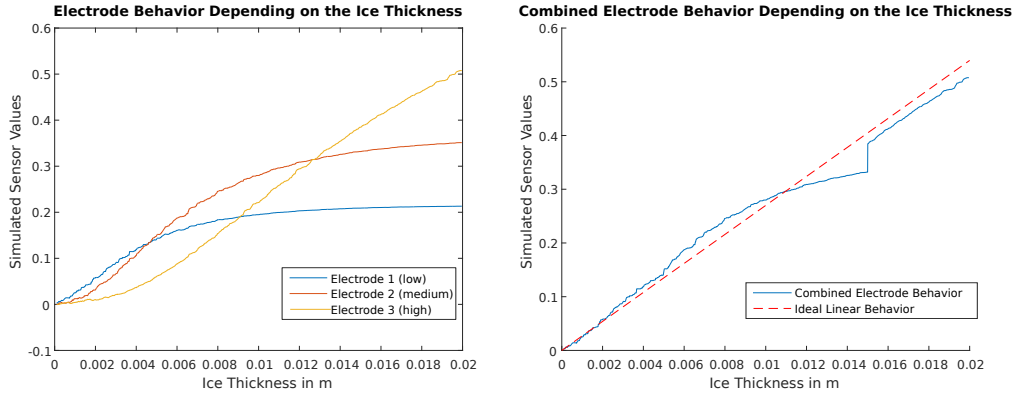


Figure 4.3: Combined linear behavior of multiple capacitances.

The measurement range is split into sub ranges, and each one is assigned to one of the electrodes of the multi-electrode sensor. A combined vector $\mathbf{C}_{\text{combined}}$ is created by

$$\mathbf{C}_{\text{combined}} = \sum_{i=1}^N \mathbf{C}_i(\mathbf{x}) \cdot u_i(\mathbf{x}), \quad (4.18)$$

using the function

$$u_i(\mathbf{x}) = \begin{cases} 1 & x_{i,\min} < x < x_{i,\max} \\ 0 & \text{else} \end{cases} \quad (4.19)$$

to define the sub ranges.

The combined vector $\mathbf{C}_{\text{combined}}$ holds the relevant simulated capacitances \mathbf{C}_i for different patterns of all N electrodes. Only the values corresponding to each electrode's range $x_{i,\min} < x < x_{i,\max}$ are combined. Then, the exact same steps as described in section 4.2 for a linear single capacitor sensor

4 Design of Optimized Sensors

are executed. In the formulae, instead of \mathbf{C} the combined capacitance vector $\mathbf{C}_{\text{combined}}$ is used.

Note that the reconstruction algorithm described for a linear single capacitor sensor would not work for a multi-capacitor sensor. The sensor does not know when to switch between the different capacitors and therefore the measurement ranges. This works in the simulation environment because the true ice thickness x is known from the pattern information. To utilize the multi-capacitor sensor, a reconstruction algorithm incorporating the information from all the electrodes like a maximum likelihood estimator, described in [26], can be used.

4.3.1 Objective Function

The MSE, described in section 4.2, is used to evaluate the performance of the linear ice sensor with multiple capacitances. Therefore, the objective function can be expressed as

$$\mathbf{v}_{\text{optimal}} = \arg \min(\text{MSE}(\mathbf{v})). \quad (4.20)$$

4.3.2 Computational Steps

This subsection describes the necessary computational steps to simulate and evaluate a linear ice sensor with multiple capacitances. Those steps will be repeated by the optimization algorithm until an optimal solution is found.

1. Create a specific sensor geometry for the sensor.
2. Simulate the sensor with numerous ice patterns corresponding to the pattern statistic.
3. Compute the combined capacitance vector $\mathbf{C}_{\text{combined}}$.
4. Determine the factor k for the linear thickness estimator.
5. Use the linear thickness estimator to compute thickness estimates \hat{x} .
6. Evaluate and return the value of the objective function.

4.4 Combined Sensor/Algorithm Design

In the combined sensor/algorithm design approach, the sensor geometry is designed together with an estimation algorithm. They can then be treated as a measurement system as illustrated in figure 3.1 and can be optimized together. A multi-capacitance sensor is used so the algorithm can combine the information from multiple electrodes.

The structure of the algorithm has to be specified. A method called Optimal Approximation is used to design a thickness estimation algorithm. It is subsequently created specifically for each new sensor. Figure 4.4 illustrates the additional step that is necessary in the optimization process.

4.4.1 Optimal Approximation as a General Estimator

Optimal Approximation is a technique to design estimation methods from sampled data [10]. It can incorporate an arbitrary number of measurement variables and evaluate their influence on the value that has to be estimated. An optimal solution is produced by minimizing the difference between the true and the estimated value. This is possible in the complete simulation process because the true values are known from the pattern information.

The estimation function f in the relation

$$\hat{x} = f(\mathbf{C}(\mathbf{x}, \mathbf{v})) \quad (4.21)$$

is not yet known but assumed to take the form

$$\hat{x} = \mathbf{p}\mathbf{h}, \quad (4.22)$$

where the vector \mathbf{p} is the reconstruction vector. The actual value for the ice thickness x is computed from the ice pattern and \hat{x} denotes the estimated ice thickness. Vector \mathbf{h} is called the augmented measurement vector and consists of the simulated sensor values C_i . Depending on the number of electrodes N , it takes the general form of

4 Design of Optimized Sensors

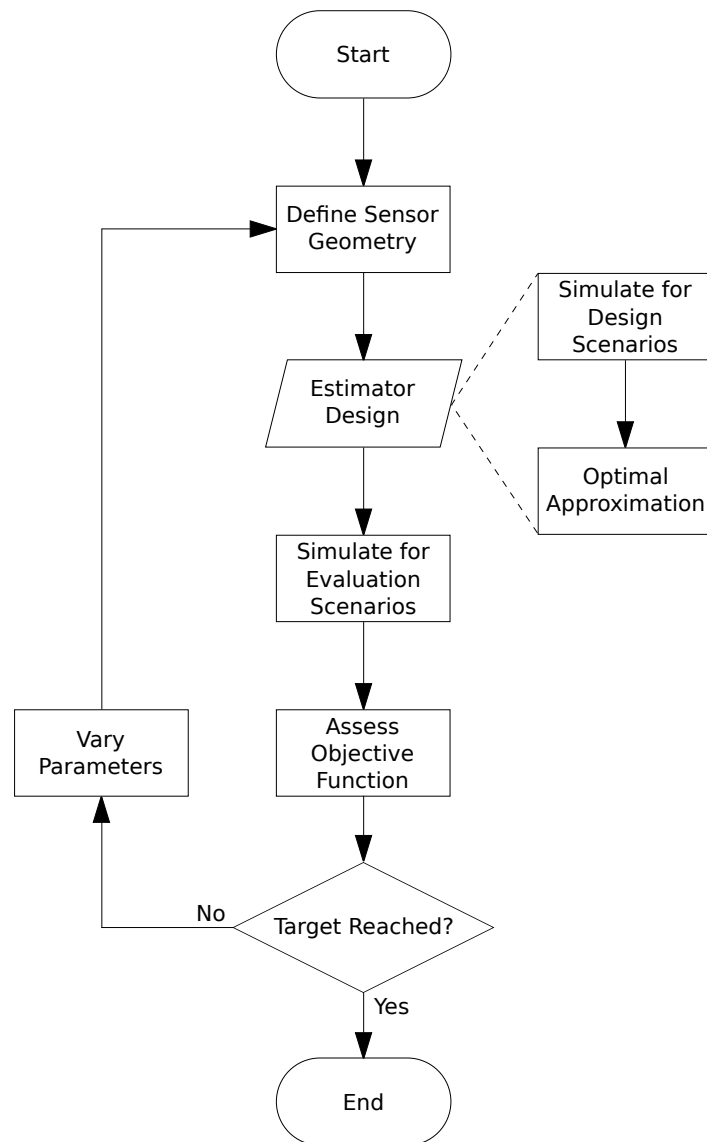


Figure 4.4: Flowchart of the optimization process, expanded by the combined sensor/algorithm design.

4.4 Combined Sensor/Algorithm Design

$$\mathbf{h} = [1 \ C_1 \ \dots \ C_i \ \dots \ C_N \ C_1^2 \ \dots \ C_i^2 \ \dots \ C_N^2]^T. \quad (4.23)$$

It is possible to include higher potentials or other functions into the vector \mathbf{h} .

To find the reconstruction vector \mathbf{p} through Optimal Approximation, the sensor is simulated with different ice patterns. The actual ice thicknesses are represented by the vector \mathbf{x} . A matrix \mathbf{H} is formed by

$$\mathbf{H} = \begin{bmatrix} \mathbf{h}_1^T \\ \vdots \\ \mathbf{h}_i^T \\ \vdots \\ \mathbf{h}_N^T \end{bmatrix}, \quad (4.24)$$

where the rows correspond to the vectors \mathbf{h}_i^T filled with the respective values from the simulations.

Using the results from many different pattern simulations creates an overdetermined system of equations. The linear least squares method can be used to find an approximate solution for

$$\mathbf{H}\mathbf{p}^T = \mathbf{x}, \quad (4.25)$$

where \mathbf{p} holds the weighing values for the reconstruction algorithm. The solution is given by

$$\mathbf{p}^T = \mathbf{H}^+ \mathbf{x}, \quad (4.26)$$

where \mathbf{H}^+ is the pseudo-inverse of \mathbf{H} . The values in \mathbf{p} are then used in formula 4.22 to produce an estimate of the ice thickness from the measured capacitance.

4 Design of Optimized Sensors

Creating the Vector of Measurement Variables

The vector \mathbf{h} for the Optimal Approximation approach can be constructed in different ways. It can hold an arbitrary number of measurement variables, their potentials, or other functions. Through computing the Optimal Approximation, the influence of each variable on the ice thickness can be determined.

The vector

$$\mathbf{h}_{\text{linear}} = [C_1 \ \dots \ C_i \ \dots \ C_N]^T \quad (4.27)$$

is used to determine the linear influence of the measured capacitances from N different electrodes C_i on the ice thickness. It can be expanded to

$$\mathbf{h}_{\text{linear+offset}} = [1 \ C_1 \ \dots \ C_i \ \dots \ C_N]^T. \quad (4.28)$$

by adding a 1 to the vector. The vector $\mathbf{h}_{\text{linear+offset}}$ can be used to determine whether there is an offset in the ice thickness that is not dependent on the capacitances C_i . It can be further expanded by also adding the squares of the measured capacitances C_i , resulting in

$$\mathbf{h}_{\text{linear+offset+squares}} = [1 \ C_1 \ \dots \ C_i \ \dots \ C_N \ C_1^2 \ \dots \ C_i^2 \ \dots \ C_N^2]^T. \quad (4.29)$$

This is done to also consider a quadratic behavior of the ice thickness.

Generally, the vector \mathbf{h} can hold any combination of measurement variables and their potentials.

4.4.2 Objective Function

Objective functions are needed to compute a measure of the sensor iteration's performance. The mean squared error (MSE) is used again like in section 4.2, represented by equation (4.13). It includes the bias as well as the variance information of the estimator. $\mathbf{v}_{\text{optimal}}$ are the optimal values for the sensor geometry and can be found by optimizing for the objective function

$$\mathbf{v}_{\text{optimal}} = \arg \min(\text{MSE}(\mathbf{v})). \quad (4.30)$$

4.4.3 Computational Steps

This subsection describes the necessary computational steps to simulate and evaluate an ice sensor with multiple capacitances, created with a combined sensor/algorithm design. Those steps will be repeated by the optimization algorithm until an optimal solution is found.

1. Create a specific sensor geometry.
2. Simulate the sensor with numerous design ice patterns corresponding to the pattern statistic.
3. Create an estimation algorithm through Optimal Approximation.
4. Simulate the sensor with numerous evaluation ice patterns corresponding to the pattern statistic.
5. Use the estimation algorithm to compute thickness estimates $\hat{\mathbf{x}}$.
6. Evaluate and return the value of the objective function.

4.5 Summary

In this section, the previous chapter on designing objective functions for the optimization of a sensor is summarized.

- A sensor can be optimized under different points of view that depend on the use case. For each use case, a separate objective function has to be formulated. It expresses the sensor's performance as a value that can be minimized by the optimization algorithm.
- The objective function for the optimization of the ice detector uses a binary classification test to assess the performance of the detector. The two cases the detector has to distinguish are ice or rain on the sensor. By calculating Youden's index, the optimal threshold to distinguish between the two cases can be found.
- For the ice thickness estimator, multiple approaches for an objective function were formulated. The linear ice sensor design optimizes the sensor for the best linear relation between sensor value and ice thickness. Each electrode was assigned a range of ice thickness and the combined behavior of all electrodes was optimized. The simple linear estimator used in the optimization cannot be used in a real world application. A maximum likelihood estimator can combine the information from multiple electrodes.
- The combined sensor/algorithm approach uses Optimal Approximation to design an optimal estimator for each sensor. The sensor electrodes and the algorithm can be treated as a measurement system and its combined behavior can be optimized.

5 Design Studies

In this chapter, the results of the different designs, featuring the approaches discussed in chapter 4, will be discussed. The design was split into two distinctive parts, the ice detector and the ice thickness sensor. Each design was optimized with the parameters for a prototype production. All optimizations done in the design studies assume that there is no measurement noise present.

The ice detector is optimized to distinguish between ice and water. Water from rain could potentially be seen by the sensor as a substantial ice layer. It is important to detect the presence of ice to assess its danger potential on a critical surface.

The ice thickness sensor is optimized for actual thickness measurement. Its thickness estimation algorithm only engages when there is actually ice on the sensor. Water on the sensor will produce false estimation results, triggering a false alarm. For the thickness sensor design there are two different approaches:

- Linear ice sensor design with multiple capacitances.
- Combined sensor/algorithm design.

Additional, the combined sensor/algorithm design will be expanded by the information about the transmitter current. Its results for different placements of the common transmitter electrode are compared.

5.1 General Prototype Considerations

The ice detector and sensor designs were optimized for the production of a prototype on a PCB. The general layout considerations and dimensions

5 Design Studies

are sketched in figure 5.1. On each PCB, an optimized layout and a hand-drawn layout are produced. This way, the performance of them can be compared by measurements.

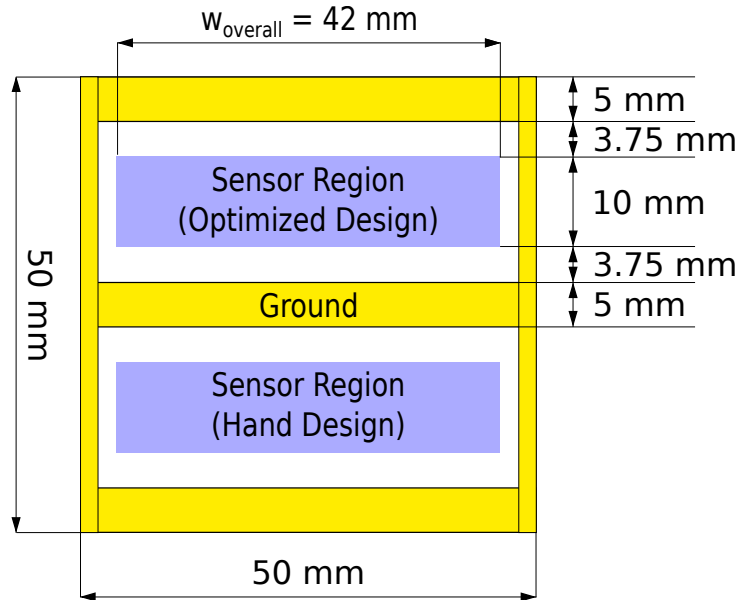


Figure 5.1: General layout of a prototype PCB.

The overall width w_{overall} of the sensor designs was chosen to be 42 mm so that the prototype could be produced on a 50 mm by 50 mm PCB with some room for shielding. Keeping the overall width w_{overall} constant for different designs makes them comparable.

The number of electrodes is limited by the number of available receiver channels of the measurement IC. All designs are made with a maximum of three receiving electrodes plus a common transmitter. This enables the evaluation of both designs, the optimized and the hand-drawn, with one sensing IC.

The properties common to all the simulations in the design studies are dependent on the production process. Parameters for a typical PCB are taken from the website of a PCB-producer [27]. Table 5.1 shows the production parameters as well as the relative permittivities for wet and frozen ice that were used.

5.2 Ice Detector Design

Table 5.1: Parameters used in the simulation process of the design studies.

Description	Symbol	Value
Copper Layer Thickness	t_{copper}	35 μm
Insulation Layer Top	$t_{\text{insulation,top}}$	160 μm
Insulation Layer Bottom	$t_{\text{insulation,bottom}}$	1.2 mm
Minimum Structure Width	w_{min}	75 μm
Minimum Structure Distance	d_{min}	75 μm
Overall Sensor Width	w_{overall}	42 mm
Maximum Ice Thickness	y_{size}	20 mm
Relative Permittivity Insulation Layer	$\epsilon_{\text{insulation}}$	4.8
Relative Permittivity Deep-Frozen Ice	$\epsilon_{\text{ice,frozen}}$	3.2
Relative Permittivity Wet Ice	$\epsilon_{\text{ice,wet}}$	7.6
Relative Permittivity Water	ϵ_{water}	80

5.2 Ice Detector Design

In this section, the design of an optimized ice detector is shown. The objective function introduced in section 4.1 is used. First simulation runs have shown that fine and narrow structures tend to produce a better distinction between ice and rain. A single capacitor in a finger structure layout shown in figure 5.2 is used.

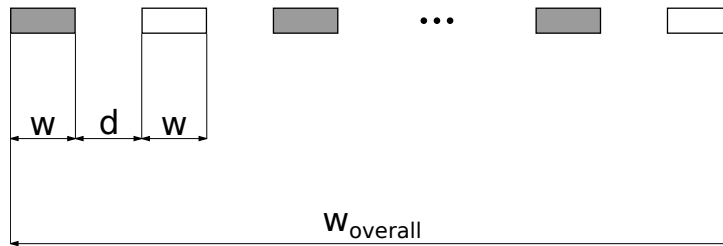


Figure 5.2: Generic model of the detector electrodes' geometries.

The basic generic model of the electrodes' geometry is depicted in figure 5.2. The sensor region with the overall width w_{overall} is filled with as many pairs of electrodes as possible. Sensing and transmitting electrode fingers share the same width w and they are all spaced out the same

5 Design Studies

distance d apart from each other. A limit for $w = 5$ mm was chosen in this design. That reduces the number of variables \mathbf{v} for the optimization algorithm to two. The vector \mathbf{v} of optimization variables can be expressed as

$$\mathbf{v} = \begin{bmatrix} w \\ d \end{bmatrix}. \quad (5.1)$$

This design study is about optimizing the sensor geometry for a binary detection algorithm. A threshold value is used to determine whether the situation on the sensor is detected as ice or rain. Youden's index J is calculated and used in the objective function for the optimization algorithm.

By using a more sophisticated algorithm, the overall performance of the detector could be improved further. For instance, it is possible to consider the variance information from a series of measurements which could identify rain by its fast-changing nature in comparison to a slow-growing ice layer.

The pattern prototype statistic that was used for the complete simulation process is:

- 30 % - Thin Film of Water of Variable Thickness (3.2.4)
- 30 % - Variable Number of Raindrops (3.2.4)
- 40 % - Thin, Wet Ice Layer of Varying Thickness Covering the Whole Sensor (3.2.5)

5.2.1 Optimization Result

Geometry Parameters

From the optimization process, the optimal geometry parameters $\mathbf{v}_{\text{optimal}}$ are given by

$$\mathbf{v}_{\text{optimal}} = \begin{bmatrix} w \\ d \end{bmatrix} = \begin{bmatrix} 4.932 \text{ mm} \\ 0.080 \text{ mm} \end{bmatrix} \quad (5.2)$$

5.2 Ice Detector Design

and the geometry parameters \mathbf{v}_{hand} for the hand designed layout by

$$\mathbf{v}_{\text{hand}} = \begin{bmatrix} w \\ d \end{bmatrix} = \begin{bmatrix} 2 \text{ mm} \\ 1 \text{ mm} \end{bmatrix}. \quad (5.3)$$

The finished layout and dimension of the optimized detector prototype are depicted in figure 5.3. On the top side of the PCB the optimized detector can be seen while a hand-drawn design will be produced on the bottom of the PCB. This is done to compare their performance in future measurements.

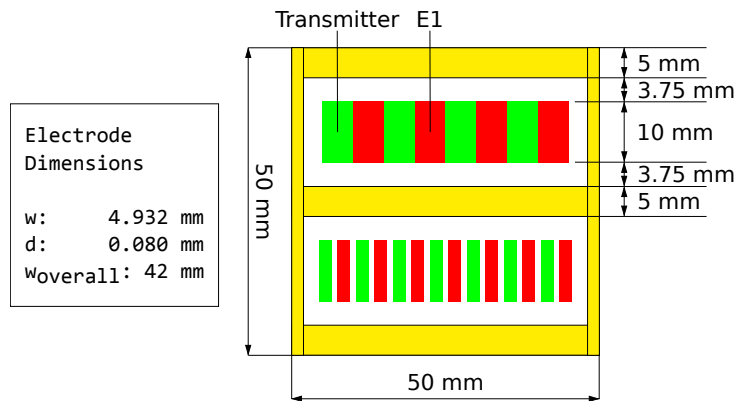


Figure 5.3: Prototype layout of the optimized detector design and a hand-drawn design.

Analysis

The ROC and Youden's index J are both methods to find the best threshold in a binary decision scenario. Details on the creation of the ROC and the calculation of Youden's index J can be found in section 4.1.1.

The ROC for the detector is plotted in 5.4. The actual best threshold value T_{rain} cannot be read from the plot. It is the threshold value that is associated with the tangent point.

Youden's index J for the result of the detector optimization is shown in table 5.2. The table also shows the performance of the hand-drawn

5 Design Studies

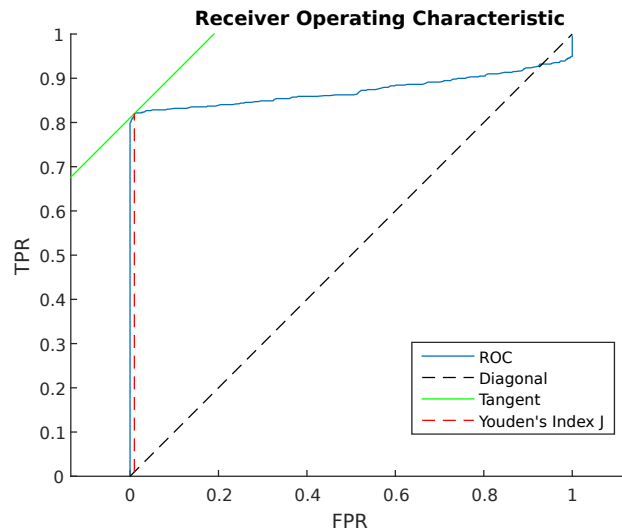


Figure 5.4: Receiver Operating Characteristic of the ice detector.

Table 5.2: Comparison of Youden's index J for different design configurations of the detector.

Nr.	Design Configuration	J
1	Optimized	0.81
2	Hand-Drawn	0.78

design for comparison. A larger Youden's index J equals a better detector performance, therefore the optimized design is better suited for ice detection.

The optimal threshold T_{rain} is then given by the threshold which resulted in the largest Youden's index J . In figure 5.5, the histograms of the simulated sensor values and the optimal threshold T_{rain} are shown. Ice and rain events are each represented by their own histograms. Ideally, they would not overlap, which would make them easily distinguishable by the detector. This is not the case with this detector, but the chosen threshold T_{rain} is the best trade-off between TPR and FPR. A definite distinction of the ice and rain scenarios is not possible. It can be concluded that a single capacitance does not provide sufficient information for an ice detector.

5.3 Linear Ice Thickness Sensor Design

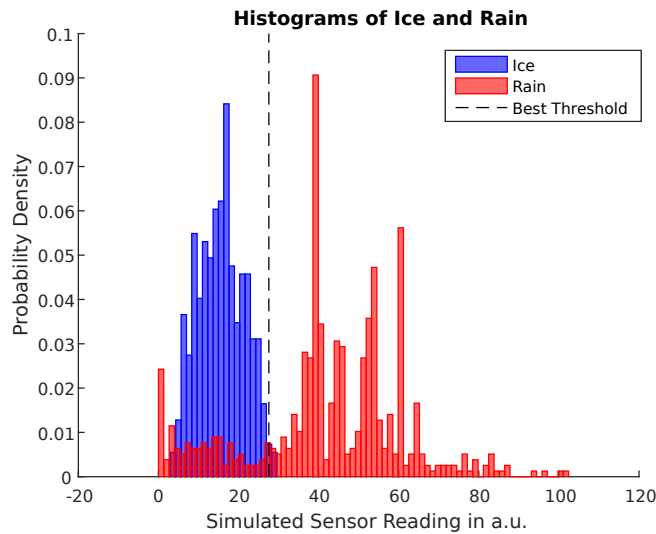


Figure 5.5: Histograms of simulated sensor values for ice and rain and the optimal threshold.

5.3 Linear Ice Thickness Sensor Design

The linear ice thickness sensor is optimized for measuring the thickness of deep-frozen, even ice layers. Even ice layers were chosen to evaluate the performance of a sensor under ideal conditions. It uses receiving electrodes of different size and distance to a common transmitter electrode. Design approaches and the objective function are described in 4.2. The combination of all the information from the single electrodes shows a better linear behavior of the ice thickness than each single electrode could. This provides a larger linear overall measurement range. A sketch of the generic sensor layout in figure 5.6 shows the three receiver electrodes as well as the common transmitter.

The widths w_i and distances d_i of the electrodes are the variables for the optimization algorithm. For three receiver electrodes, this amounts to seven variables. The electrodes have to fill the whole sensor region with the overall width w_{overall} . Therefore, the sum of all widths w_i and distances d_i has to be w_{overall} . The vector \mathbf{v} of optimization variables can be expressed as

5 Design Studies

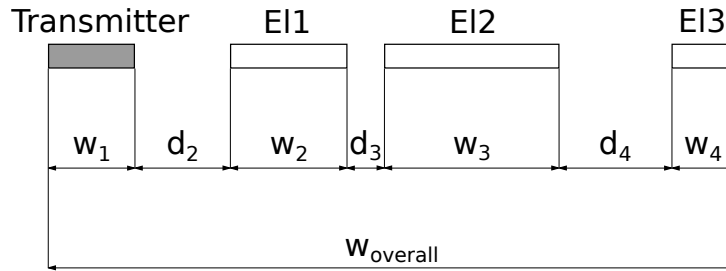


Figure 5.6: Generic model of the sensing electrodes' geometries.

$$\mathbf{v} = \begin{bmatrix} w_1 \\ d_2 \\ w_2 \\ d_3 \\ w_3 \\ d_4 \\ w_4 \end{bmatrix}. \quad (5.4)$$

For the combination of the capacitance values described in section 4.3, the measurement range of the ice thickness $y_{\text{size}} = 20 \text{ mm}$ was split into three sub-ranges. Each sub-range was assigned to an electrode:

- Electrode 1: 0 mm – 5 mm
- Electrode 2: 5 mm – 15 mm
- Electrode 3: 15 mm – 20 mm

The linear sensor was optimized for an ideal scenario where deep-frozen ice covers the sensor evenly. Therefore, the pattern prototype statistic that was used for the complete simulation process is:

- 100% - Deep-Frozen Ice Layer of Varying Thickness Covering the Whole Sensor (3.2.5)

5.3.1 Optimization Result

Geometry Parameters

The optimal geometry parameters $\mathbf{v}_{\text{optimal}}$ found by the optimization algorithm are given by

$$\mathbf{v}_{\text{optimal}} = \begin{bmatrix} w_1 \\ d_2 \\ w_2 \\ d_3 \\ w_3 \\ d_4 \\ w_4 \end{bmatrix} = \begin{bmatrix} 0.761 \text{ mm} \\ 17.533 \text{ mm} \\ 0.510 \text{ mm} \\ 4.719 \text{ mm} \\ 4.175 \text{ mm} \\ 1.265 \text{ mm} \\ 13.037 \text{ mm} \end{bmatrix} \quad (5.5)$$

and the geometry parameters \mathbf{v}_{hand} for the hand-drawn layout by

$$\mathbf{v}_{\text{hand}} = \begin{bmatrix} w_1 \\ d_2 \\ w_2 \\ d_3 \\ w_3 \\ d_4 \\ w_4 \end{bmatrix} = \begin{bmatrix} 8 \text{ mm} \\ 2 \text{ mm} \\ 5 \text{ mm} \\ 3 \text{ mm} \\ 8 \text{ mm} \\ 1 \text{ mm} \\ 15 \text{ mm} \end{bmatrix} . \quad (5.6)$$

A drawing of the layout with its dimensions is depicted in figure 5.7.

Analysis

In this subsection, the results for the linear ice thickness sensor evenly covered by deep-frozen ice are shown. Since the proportionality factor k is known from the simulations, the estimated ice thickness can be calculated from the capacitances C_i .

Figure 5.8 depicts the behavior of the estimates for the three electrodes and the measurement-sub-ranges. It can be seen that the electrodes do

5 Design Studies

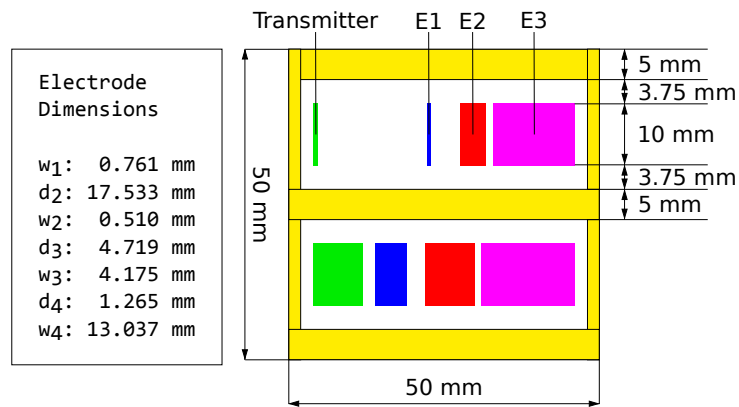


Figure 5.7: Prototype layout of the optimized linear ice thickness sensor design and a hand-drawn design.

not behave linearly outside of their sub-ranges they are dedicated to. The combined behavior is depicted in figure 5.9, together with the ideal linear behavior.

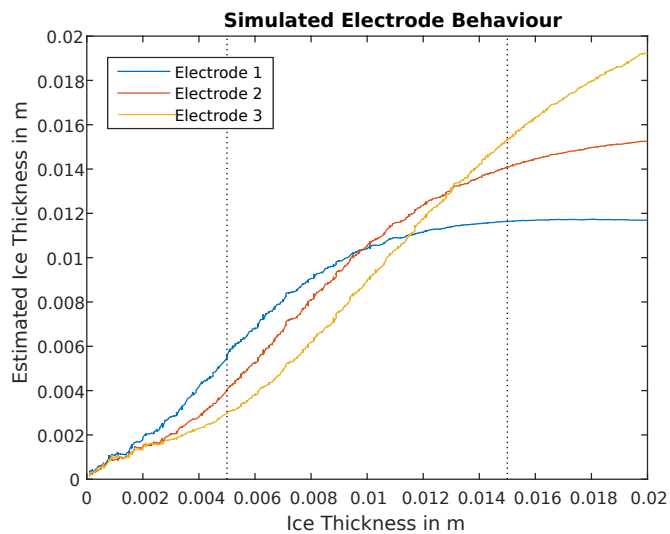


Figure 5.8: Simulated electrode behavior depending on the ice thickness (optimized).

Figure 5.10 depicts the combined behavior of the electrodes of the hand-drawn design. It can be seen that the individual capacitances do not behave linearly in their corresponding sub-range.

5.3 Linear Ice Thickness Sensor Design

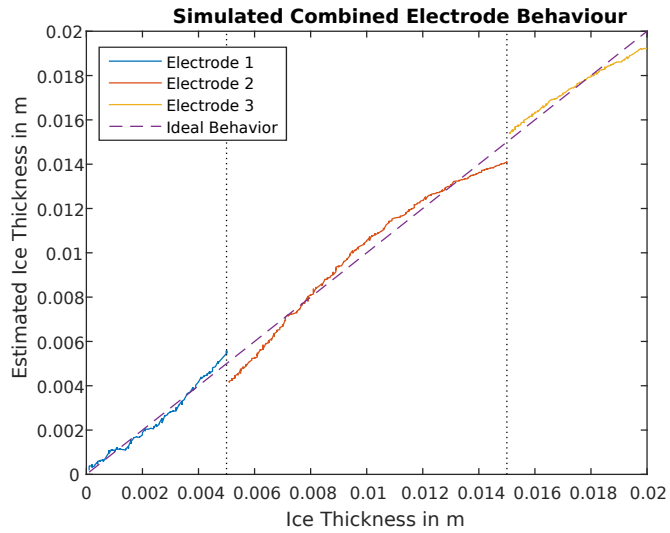


Figure 5.9: Simulated combined electrode behavior depending on the ice thickness (optimized).

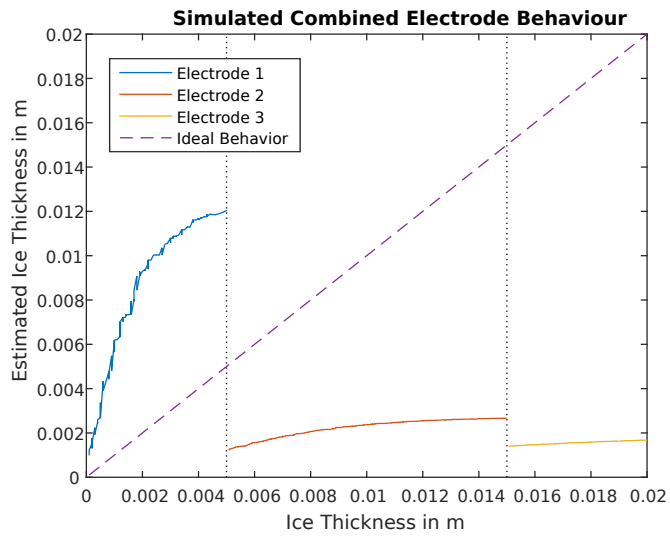


Figure 5.10: Simulated electrode behavior depending on the ice thickness (hand-drawn).

5 Design Studies

Table 5.3: Comparison of the MSE for different configurations of the linear sensor design.

Nr.	Design Configuration	MSE
1	Optimized	$155 \cdot 10^{-9}$
2	Hand-Drawn	$105 \cdot 10^{-6}$

The table 5.3 shows a comparison of the MSE-values for the optimized and the hand-drawn design, where a lower MSE equals a more linear behavior.

Note that the linear reconstruction algorithm cannot be used outside of a simulation environment for multiple electrodes. This is because a real world sensor has no access to the real thickness values x to decide which electrode's information to use. An algorithm that can combine the information from multiple electrodes, like the maximum likelihood estimator, is needed [26].

5.4 Combined Sensor/Algorithm Design

The combined sensor/algorithm design described in section 4.4 is a more rigorous approach to sensor design. It treats the sensor and the estimation algorithm as a unit and optimizes them together. Different pattern prototypes are used to create a wide range of possible icing scenarios. In contrast to ideal ice formation used in section 5.3, this will optimize the sensor for use in non-ideal, randomized conditions.

The results of selecting another position for the common transmitter electrode are compared. Additionally, the effects of adding the transmitter current information to the reconstruction algorithm are analyzed.

The generic sensor geometry for the combined sensor/algorithm design is sketched in figure 5.6. Since the design also uses three electrodes in addition to the common transmitter, the generic sensor geometry is the same as in section 5.3. The same vector of geometry parameters \mathbf{v} is also used and shown in equation (5.4).

5.4 Combined Sensor/Algorithm Design

For the Optimal Approximation method, described in subsection 4.4.1, the vector \mathbf{h} has to be chosen. In this design study it is defined as

$$\mathbf{h} = [1 \ C_1 \ C_2 \ C_3 \ C_1^2 \ C_2^2 \ C_3^2 \ C_1^3 \ C_2^3 \ C_3^3]^T. \quad (5.7)$$

The pattern prototype statistic for the optimization was:

- 10% - Deep-Frozen Ice Layer of Varying Thickness Covering the Whole Sensor (3.2.5)
- 18% - Wet Ice Layer of Varying Thickness Covering the Whole Sensor (3.2.5)
- 18% - Deep-Frozen Ice of Varying Thickness Covering Half the Sensor (3.2.5)
- 18% - Wet Ice of Varying Thickness Covering Half the Sensor (3.2.5)
- 18% - Wet Ice of Varying Thickness Unevenly Covering the Sensor (3.2.5)
- 18% - Thin, Wet Ice Layer of Varying Thickness Covering the Whole Sensor (3.2.5)

5.4.1 Transmitter Current Consideration

For a possible expansion in a later iteration of the sensor prototype, the influence of the transmitter current on the performance of the ice sensor was analyzed too. The transmitter current is proportional to the self-capacitance of the transmitter electrode [28]. It was evaluated whether this holds any relevant information about the ice layer thickness. A new measurement IC with the ability to also monitor the transmitter current would be needed to include this information in a real sensor.

In the simulation environment, it is easy to include the self-capacitance of the transmitter C_{trans} in the design of the optimal estimator. The objective function of the combined sensor/algorithm design approach can be expanded by adding a new element C_{trans} to the vector

$$\mathbf{h}_{\text{trans}} = [1 \ C_1 \ C_2 \ C_3 \ C_1^2 \ C_2^2 \ C_3^2 \ C_1^3 \ C_2^3 \ C_3^3 \ C_{\text{trans}}]^T \quad (5.8)$$

5 Design Studies

to describe the transmitter current. By using the optimal approximation approach described in 4.4.1, it can be determined whether the transmission current has an influence on the estimation result of the ice thickness.

5.4.2 Optimization Result

Geometry Parameters

The optimal geometry parameters $\mathbf{v}_{\text{optimal}}$ are those for the electrode setup with the common transmitter on the first position and without considering the transmitter current in the optimization. They are given by

$$\mathbf{v}_{\text{optimal}} = \begin{bmatrix} w_1 \\ d_2 \\ w_2 \\ d_3 \\ w_3 \\ d_4 \\ w_4 \end{bmatrix} = \begin{bmatrix} 4.736 \text{ mm} \\ 7.635 \text{ mm} \\ 7.653 \text{ mm} \\ 0.578 \text{ mm} \\ 14.037 \text{ mm} \\ 6.975 \text{ mm} \\ 0.386 \text{ mm} \end{bmatrix}, \quad (5.9)$$

and the PCB-layout is depicted in figure 5.11.

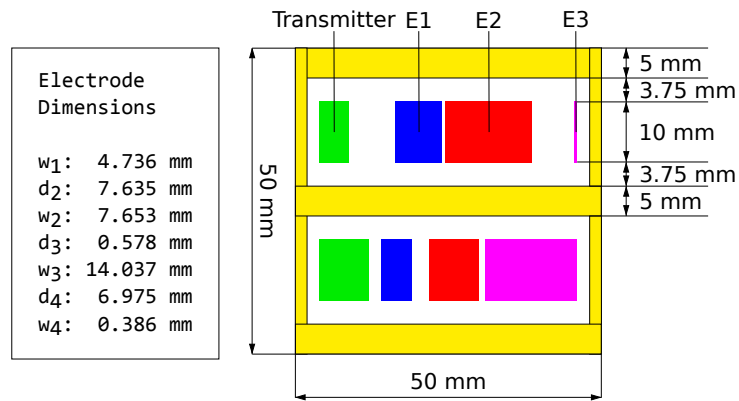


Figure 5.11: Prototype layout of the ice thickness sensor optimized by the combined sensor/algorithm design and a hand-drawn design.

5.4 Combined Sensor/Algorithm Design

The same hand-drawn layout as in section 5.3 is used and therefore its geometry parameters \mathbf{v}_{hand} are the same as in equation (5.6).

Analysis

The plot in figure 5.12 shows the mean performance of the combination of sensor and estimation algorithm. The values represent the average over all estimated values \hat{x} for the same true ice thickness x . All true thickness values were rounded to the nearest multiple of 0.1 mm to calculate the average.

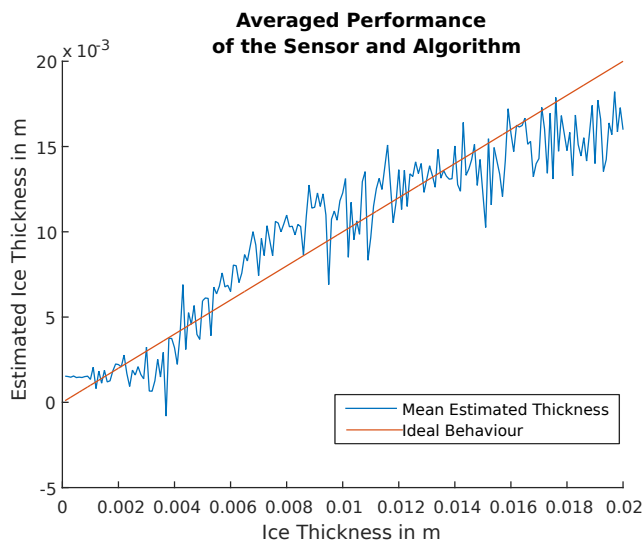


Figure 5.12: Averaged performance of the sensor and algorithm.

Figure 5.13 depicts the linear fitted performance of the sensor. Each dot in the plot represents the estimated thickness value \hat{x} of a single simulation with a random ice pattern. The polynomial fit for the estimated thicknesses \hat{x} reveals a slight bias. Where the fitted line crosses the ideal line at an ice thickness of $x = 7$ mm, the sensor is expected to perform best.

Figure 5.14 plots the standard deviation of the estimated thickness values \hat{x} . All true thickness values x were rounded to the nearest multiple of 1 mm to calculate the average. A finer resolution of the thickness results

5 Design Studies

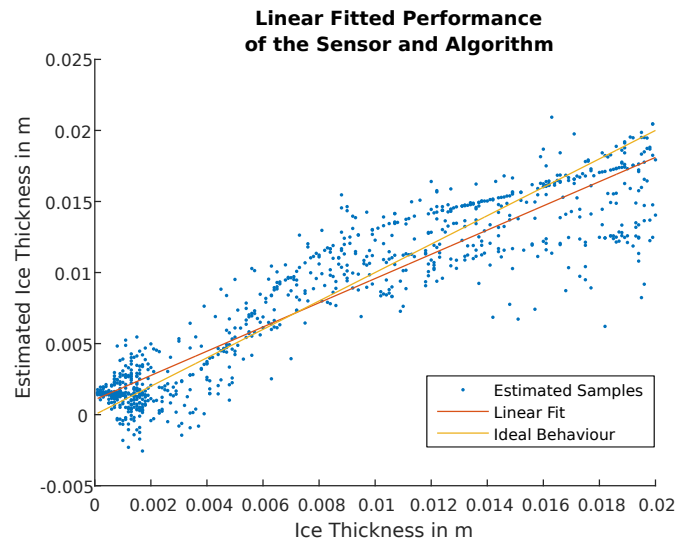


Figure 5.13: Linear fit to the performance of the sensor and algorithm.

in a very cluttered plot. The standard deviation is increasing with the ice thickness. This indicates a better sensor performance for thinner layers.

Table 5.4 compares the different configurations that were optimized with the combined sensor/algorithm design with the hand-drawn design. A lower MSE equals a better performance. It can be seen that the position of the common transmitter electrode has an influence on the performance. This encourages the optimization and comparison of all possible combinations to find the best result. For four electrodes in total, these two cases are all reasonable possible permutations. Choosing position 3 or 4 for the common transmitter produces the mirrored configurations of choosing position 2 or 1 and therefore the same sensor design. Including the transmitter current information also leads to an overall improved ice estimation.

5.4 Combined Sensor/Algorithm Design

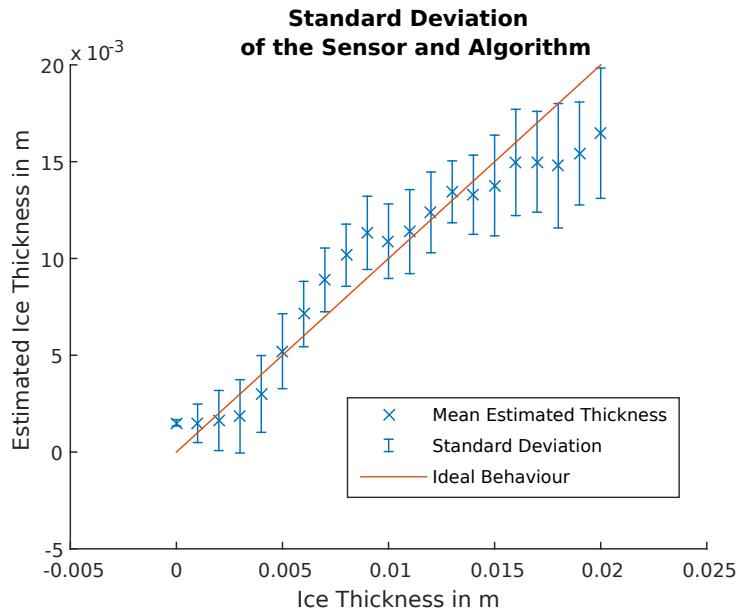


Figure 5.14: Standard deviation of the sensor and algorithm.

Table 5.4: Comparison of the MSE for different configurations of the combined sensor/algorithm design.

Nr.	Design Configuration	MSE
1	Optimized, Transmitter Position 1	$5.63 \cdot 10^{-6}$
2	Optimized, Transmitter Position 2	$6.22 \cdot 10^{-6}$
3	Optimized, Transmitter Position 1, Transmitter Current	$4.87 \cdot 10^{-6}$
4	Hand-Drawn, Transmitter Position 1	$8.72 \cdot 10^{-6}$

6 Conclusion and Outlook

6.1 Conclusion

This thesis was motivated by the need for a sensing system for ice accretion on technical structures that operate outdoors in cold climate regions. The additional mass on the critical surfaces can pose a threat to those technical structures and to people alike. Sensing systems are needed to detect the presence of ice and measure its mass. This information is used to assess the risks and damage potentials. A capacitive approach to ice sensing was chosen because it has already been proven viable. This thesis analyzes the potential for improvement by optimizing the capacitive sensing electrode geometry and the placement of electrodes in a multi-electrode configuration.

Capacitive sensing of ice poses the challenge of an indirect measurement. The properties of ice that are of interest do not generally directly correspond to the capacitance. A thin water film from rain on the sensor can result in the same capacitance value as a more substantial ice layer, introducing an uncertainty to the indirect measurement.

The dielectric properties of ice are of special interest for the capacitive sensing approach because they directly influence the capacitance. Ice shows a substantial dependence on the environmental factors in that regard. Its permittivity changes with respect to the content of unfrozen water due to the state of freezing. The behavior of ice under those circumstances was analyzed.

Different ice and rain scenarios had to be investigated to compare and understand them. In nature, ice accretion is not a perfectly ideal, deter-

6 Conclusion and Outlook

ministic process, but shows a rather random behavior. The distribution of raindrops can also be considered a stochastic process.

All results from the analysis of ice were incorporated into a framework for simulating the behavior of a sensor for different ice and rain scenarios. The framework provides a general model for the sensor as well as a method to represent the irregular nature of ice and rain.

Results from the simulation of a sensor can be used in an optimization process to find a sensor with suitable properties in regard to ice sensing or detection. Different objective functions which are used to formulate which properties and behaviors are considered suitable were discussed. Each one represents a different approach to designing an optimal sensor. The evaluation of a sensor's performance had to take the random nature or the scenarios into consideration by employing tools of statistical analysis.

The framework was then used to produce sensor designs for the different objective functions. They were evaluated and compared against a hand-drawn design. It was shown that the optimized designs perform better than the hand-drawn designs with respect to the objective function.

The promising results of the optimized sensor designs as well as the methods implemented in the framework constitute an essential building block for future further research in this field.

6.2 Outlook

6.2.1 Confirmation of the Simulation Results and Construction of a Prototype

Comparisons between the simulations and the measurements of the prototype capacitive ice sensor have shown similar behavior. The results of sensor simulations created with the framework still need to be compared against measurements. Because new measurement electronics have to be designed, this is beyond the scope of this thesis. Modifications to the model can easily be done because of the modular structure of the framework.

There are numerous aspects that have to be considered in the construction of a sensor prototype from the optimization results. One possibility would be a flat PCB as described in the chapter 5 on design studies. The sensor could also be produced on the surface of a tube which is then mounted on the power transmission line.

6.2.2 Different Objective Functions

The performance of the sensor that is created by the framework substantially relies on the formulation of the objective function. Sensor designs will be an optimized solution for the specific objective function that was used. To design a meaningful objective function is a complicated task with a lot of possible approaches to consider.

For instance, when formulating the combined sensor/algorithm approach, a specific type of recreation algorithm was used. Other, more complex solutions might be employed for improved results.

A different objective function for the ice detector would not only use a threshold to distinguish between the scenarios. With the current approach, each simulation is a snapshot of a randomized ice or rain scenario. The simulation results are evaluated with statistical methods, but there is no way to represent the evolution of a scenario over time. For instance, ice accretion could be considered a slowly changing process where each

6 Conclusion and Outlook

scenario is correlated to its predecessor scenario. The implementation of this behavior would require changes to the general framework.

6.2.3 Deeper Study of Ice Patterns

The patterns of ice scenarios that were used in the simulation framework were based on observations. They were made in the course of taking measurements in the climatic chamber and cover a variety of generic cases. Those patterns might not necessarily also occur in outside weather conditions. On the other hand, there are scenarios that did not occur under laboratory conditions and are not included in the framework. The probabilities with which patterns occur in nature, and their influence on the optimization have not been investigated.

Bibliography

- [1] D. O. Koval and A. A. Chowdhury, "An investigation into extreme-weather-caused transmission line unavailability," in *IEEE Power Engineering Society General Meeting, 2005*, Jun. 2005, 2425–2428 Vol. 3. DOI: 10.1109/PES.2005.1489270 (cit. on p. 1).
- [2] M. Farzaneh and K. Savadjiev, "Statistical analysis of field data for precipitation icing accretion on overhead power lines," *IEEE Transactions on Power Delivery*, vol. 20, no. 2, pp. 1080–1087, Apr. 2005, ISSN: 0885-8977. DOI: 10.1109/TPWRD.2004.838518 (cit. on p. 1).
- [3] M. Lacavalla, P. Marcacci, and A. Frigerio, "Forecasting and monitoring wet-snow sleeve on overhead power lines in Italy," in *Environmental, Energy and Structural Monitoring Systems (EESMS), 2015 IEEE Workshop on*, Jul. 2015, pp. 78–83. DOI: 10.1109/EESMS.2015.7175856 (cit. on p. 1).
- [4] Z. Peter, M. Farzaneh, and L. I. Kiss, "Assessment of the Current Intensity for Preventing Ice Accretion on Overhead Conductors," *IEEE Transactions on Power Delivery*, vol. 22, no. 1, pp. 565–574, Jan. 2007, ISSN: 0885-8977. DOI: 10.1109/TPWRD.2006.877091 (cit. on p. 2).
- [5] Y. Liu, X. Yin, J. Xu, and Z. Li, "Mechanical monitoring and risk assessment under ice disaster based on wireless sensor network," in *Power Engineering and Automation Conference (PEAM), 2011 IEEE*, vol. 2, Sep. 2011, pp. 229–232. DOI: 10.1109/PEAM.2011.6134944 (cit. on p. 3).

Bibliography

- [6] X. Yundong and L. Jinying, "Study on the icing process of transmission lines and the local meteorological parameters," in *CICED 2010 Proceedings*, Sep. 2010, pp. 1–4. [Online]. Available: <http://ieeexplore.ieee.org/document/5736092/?arnumber=5736092> (cit. on p. 3).
- [7] G. Xin, X. Jin, and H. Xiaoguang, "On-line monitoring system of transmission line icing based on DSP," in *2010 5th IEEE Conference on Industrial Electronics and Applications*, Jun. 2010, pp. 186–190. DOI: 10.1109/ICIEA.2010.5516756 (cit. on p. 3).
- [8] W. Li, J. Zhang, L. Ye, and C. Li, "Modelling and experimental study on the fiber-optic ice sensor," in *Information and Automation, 2009. ICIA '09. International Conference on*, Jun. 2009, pp. 1298–1301. DOI: 10.1109/ICINFA.2009.5205117 (cit. on p. 3).
- [9] L. K. Baxter, "Capacitive Sensor Basics," in *Capacitive Sensors: Design and Applications*. Wiley-IEEE Press, 1997, pp. 37–47, ISBN: 9780470544228. DOI: 10.1109/9780470544228.ch3 (cit. on pp. 3, 4, 78).
- [10] M. Neumayer, H. Zangl, D. Watzenig, and A. Fuchs, "Current Reconstruction Algorithms in Electrical Capacitance Tomography," in *New Developments and Applications in Sensing Technology*, S. C. Mukhopadhyay, A. Lay-Ekuakille, and A. Fuchs, Eds. Berlin, Heidelberg: Springer Berlin Heidelberg, 2011, pp. 65–106, ISBN: 978-3-642-17943-3. DOI: 10.1007/978-3-642-17943-3_4 (cit. on pp. 5, 87).
- [11] M. J. Moser, B. George, H. Zangl, and G. Brasseur, "Icing detector for overhead power transmission lines," in *Instrumentation and Measurement Technology Conference, 2009. I2MTC '09. IEEE*, May 2009, pp. 1105–1109. DOI: 10.1109/IMTC.2009.5168619 (cit. on pp. 6, 7).
- [12] T. Bretterkieber, M. Neumayer, M. Flatscher, A. Becke, and G. Brasseur, "Model based monitoring of ice accretion on overhead power lines," in *2016 IEEE International Instrumentation and Measurement Technology Conference Proceedings*, May 2016, pp. 1–6. DOI: 10.1109/I2MTC.2016.7520468 (cit. on pp. 6–9, 13, 22).

- [13] H. Zangl, "Capacitive sensors uncovered: Measurement, detection and classification in open environments," *Procedia engineering*, vol. 5, pp. 393–399, 2010, ISSN: 1877-7058. DOI: 10.1016/j.proeng.2010.09.130 (cit. on p. 13).
- [14] L. K. Baxter, "Electrostatics," in *Capacitive Sensors: Design and Applications*. Wiley-IEEE Press, 1997, pp. 6–36, ISBN: 9780470544228. DOI: 10.1109/9780470544228.ch2 (cit. on p. 14).
- [15] M. Neumayer, *3D-ECT Simulation Framework*, Apr. 1, 2015 (cit. on pp. 14, 70).
- [16] Analog Devices. (Sep. 26, 2016). Programmable Controller for Capacitance Touch Sensor AD7143, [Online]. Available: www.analog.com/media/en/technical-documentation/data-sheets/AD7143.pdf (cit. on p. 21).
- [17] The Engineering ToolBox. (Sep. 26, 2016). Relative Permittivity - the Dielectric Constant, [Online]. Available: www.engineeringtoolbox.com/relative-permittivity-d_1660.html (cit. on pp. 25, 37).
- [18] W. Ellison, K. Lamkaouchi, and J.-M. Moreau, "Water: A dielectric reference," *Journal of Molecular Liquids*, vol. 68, no. 2, pp. 171–279, 1996, ISSN: 0167-7322. DOI: 10.1016/0167-7322(96)00926-9 (cit. on p. 25).
- [19] Y. Zhao, Y. Chen, L. Tong, L. Zhong, and M. Jia, "The Measurement on the Dielectric Properties of Fresh-Water Ice with Rectangular Waveguide at 2.6 GHz-3.9 GHz," in *IGARSS 2008 - 2008 IEEE International Geoscience and Remote Sensing Symposium*, vol. 4, Jul. 2008, pp. 1165–1168. DOI: 10.1109/IGARSS.2008.4779935 (cit. on p. 35).
- [20] L. Jared West, D. M. Rippin, T. Murray, H. M. Mader, and B. Hubbard, "Dielectric Permittivity Measurements on Ice Cores: Implications for Interpretation of Radar to Yield Glacial Unfrozen Water Content," *Journal of Environmental & Engineering Geophysics*, vol. 12, no. 1, pp. 37–45, 2007, ISSN: 1083-1363. DOI: 10.2113/JEEG12.1.37 (cit. on p. 35).

Bibliography

- [21] S. D. Hannot, D. J. Rixen, and V. Rochus, "Rounding the Corners in an Electromechanical FEM Model," in *Int. Conf. on Computational Methods for Coupled Problems in Science and Engineering, 2007, 2007* (cit. on p. 52).
- [22] J. R. Shewchuk. (Sep. 26, 2016). Triangle A Two-Dimensional Quality Mesh Generator and Delaunay Triangulator. Version 1.6, [Online]. Available: www.cs.cmu.edu/~quake/triangle.html (cit. on p. 70).
- [23] K. Price and R. Storn. (Sep. 26, 2016). Differential Evolution for Continuous Function Optimization, [Online]. Available: www1.icsi.berkeley.edu/~storn/code.html (cit. on p. 73).
- [24] S. M. Kay, *Fundamentals of Statistical Signal Processing, Volume II: Detection theory*, ser. Fundamentals of Statistical Signal Processing Bd. 2. Prentice-Hall PTR, 1998, ISBN: 978-0-13-504135-2 (cit. on p. 79).
- [25] W. J. Youden, "Index for rating diagnostic tests," *Cancer*, vol. 3, no. 1, pp. 32–35, 1950, ISSN: 1097-0142. DOI: 10.1002/1097-0142(1950)3:1<32::AID-CNCR2820030106>3.0.CO;2-3 (cit. on p. 80).
- [26] S. M. Kay, *Fundamentals of Statistical Signal Processing, Volume I: Estimation theory*, ser. Fundamentals of Statistical Signal Processing Bd. 1. Prentice-Hall PTR, 1993, ISBN: 978-0-13-345711-7 (cit. on pp. 86, 104).
- [27] Multi Circuit Boards Ltd. (Sep. 26, 2016). Multi-cb Leiterplatten, [Online]. Available: www.multi-circuit-boards.eu/index.html (cit. on p. 94).
- [28] T. Schlegl and H. Zangl, "Sensor Interface for Multimodal Evaluation of Capacitive Sensors," *Journal of Physics: Conference Series*, vol. 450, no. 1, p. 012 018, Jun. 2013. DOI: 10.1088/1742-6596/450/1/012018 (cit. on p. 105).